Simulation of the effects of low volatility organic compounds on aerosol number concentrations in Europe

David Patoulias[1,2] and Spyros N. Pandis[1,2]

[1] Department of Chemical Engineering, University of Patras, Patras, Greece

[2] Institute of Chemical Engineering Sciences, Foundation for Research and Technology – Hellas (FORTH/ICE-HT), Patras, Greece

Corresponding author: Spyros Pandis (spyros@chemeng.upatras.gr)

Abstract

PMCAMx-UF, a three-dimensional chemical transport model focusing on the simulation of the ultrafine particle size distribution and composition has been extended with the addition of reactions of chemical aging of semi-volatile anthropogenic organic vapors, the emissions and chemical aging by intermediate volatile organic compounds (IVOCs) and the production of extremely low volatility organic compounds (ELVOCs) by monoterpenes. The model is applied in Europe to quantify the effect of these processes on particle number concentrations. The model predictions are evaluated against both ground measurements collected during the PEGASOS 2012 summer campaign across many stations in Europe and airborne observations by a Zeppelin measuring above Po-Valley, Italy. PMCAMx-UF reproduces the ground level daily average concentrations of particles with diameter larger than 100 nm (N_{100}) with normalized mean error (NME) of 45% and normalized mean bias (NMB) close to 10%. For the same simulation, PMCAMx-UF tends to overestimate the concentration of particles larger with diameter than 10 nm (N_{10}) with a daily NMB of 23% and a daily NME of 63%. The model was able to reproduce more than 75% of the N_{10} and N_{100} airborne observations (Zeppelin) within a factor of 2.

According to the PMCAMx-UF predictions, the ELVOC production by monoterpenes leads to surprisingly small changes of the average number concentrations over Europe. The total number concentration decreased due to the ELVOC formation by 0.2%, the N_{10} decreased by 1.1%, while N_{50} (particles with diameter larger than 50 nm) increased by 3% and N_{100} by 4% due to this new

secondary organic aerosol (SOA) source. This small change is due to the nonlinearity of the system with increases predicted in some areas and decreases in others, but also the cancelation of the effects of the various processes like accelerated growth and accelerated coagulation. Locally, the effects can be significant. For example, an increase in N_{100} by 20-50% is predicted over Scandinavia and significant increases (10-20%) over some parts of central Europe. The ELVOCs contributed on average around 0.5 μg m^{-3} and accounted for 10-15% of the PM$_{2.5}$ OA. The addition of IVOC emissions and their aging reactions led to surprising reduction of the total number of particles (N_{tot}) and N_{10} by 10-15 and 5-10%, respectively, and to an increase of the concentration of N_{100} by 5-10%. These were due to the accelerated coagulation and reduced nucleation rates.

1. Introduction

Two major processes are responsible for the introduction of new particles in the atmosphere: direct emission from numerous sources and nucleation from low-volatility vapors. New particles formed by nucleation can either grow by condensation of vapors (e.g. sulfuric acid, ammonia, nitric acid, and organics) to larger sizes becoming cloud condensation nuclei (CCN) and thereby may increase the cloud droplet number concentration (CDNC) or affected by coagulation with pre-existing larger particles and be lost (Adams and Seinfeld, 2002). Globally, according to large-scale model simulations, atmospheric new particle formation (NPF) and subsequent particle growth represent the most significant source of atmospheric aerosol particles, at least in terms of their total number concentration (Kulmala et al., 2004; Makkonen et al., 2009; Merikanto et al., 2009; Pierce and Adams, 2009; Wang and Penner, 2009; Yu and Luo, 2009). An increase of the number concentration of particles that may act as CCN results in higher CDNC and brighter clouds with longer lifetimes.

Globally, organic particulate matter makes up more than 50% of the sub-micrometer mass concentration of ambient aerosols in locations throughout the world (Kanakidou et al., 2005; Seinfeld and Pandis, 2006; Zhang et al., 2007). Nearly 70% of this material is thought to be secondary organic aerosol (SOA) formed from the oxidation of volatile organic compounds (VOCs) (Hallquist et al., 2009; Schulze et al., 2017). Many of the relevant precursor VOCs are biogenic in origin, such as monoterpenes ($C_{10}H_{16}$) and isoprene (C_5H_8).

Several recent field studies have shown that SOA in polluted areas cannot be explained by the simulation of only the first generation of reactions of "traditional" SOA precursors: biogenic

compounds (monoterpenes, sesquiterpenes, and isoprene) and anthropogenic compounds (aromatics, olefins and large alkanes) (de Gouw et al., 2005; Volkamer et al., 2006; Kleinman et al., 2008; Docherty et al., 2008; Matsui et al., 2009; Dzepina et al., 2009). At the same time, it has become clear that organic vapors are responsible for most of the new particle growth in environments with low sulfur dioxide levels (Olenius et al., 2018; Yli-Juuti et al., 2020).

Traditional treatment of SOA formation considers only VOCs as the precursors and only semivolatile products (Odum et al., 1996). Robinson et al. (2007) suggested that intermediate volatile organic compounds (IVOCs) either emitted directly or resulting from the evaporation of particles may be an important and previously neglected pool of precursors for SOA formation. In addition, later generations of reactions of the products of VOCs, IVOCs and SVOCs can lead to products of even lower volatility and formation of SOA (Donahue et al., 2006). These chemical reactions can lead to continued SOA production after complete precursor consumption as products undergo further oxidation (Kroll et al, 2006; Ng et al., 2006).

Secondary extremely low volatile organic compounds (ELVOCs) have been detected both in the ambient atmosphere and laboratory studies (Donahue et al., 2011). These compounds promote new particle growth and CCN production in the atmosphere (Jokinen et al., 2015; Kirkby et al., 2016). ELVOCs can be produced rapidly in the gas phase during monoterpene oxidation (Ehn et al., 2014), and can enhance atmospheric new particle formation and growth (Jokinen et al., 2015). Due to their exceptionally low volatility, ELVOCs condense essentially irreversibly onto growing particles at a rate controlled by the Fuchs-adjusted particle surface area (Shrivastava et al., 2017). The addition of the ELVOCs in PMCAMx-UF increased the effective biogenic SOA yields, becoming an additional source of SOA especially significant at low OA levels. At the same time, the addition of this extra material results in a change in the volatility distribution of the predicted SOA.

Fanourgakis et al. (2019) evaluated 16 global chemistry transport models during a 4-year period and compared their prediction to the near-surface observed number concentration of aerosol particles across Europe and Japan. All models tended to underestimate the number concentrations for particles larger with diameter than 50 nm (N_{50}). The normalized mean bias (NMB) was -51% and normalized mean error (NME) was 55% for all stations. Sengupta et al. (2021) used the GLOMAP (Global Model of Aerosol Processes; Spracklen et al., 2005) modal aerosol microphysics model (Mann et al., 2010) simulating the production of six surrogate SOA species

from the oxidation of anthropogenic VOCs, monoterpenes, and isoprene. It was assumed that ELVOCs derive only from biogenic sources and can nucleate to form new particles (Gordon et al., 2016). Different values of the ELVOC yield were used and the model predictions were compared to observations of OA mass concentration as well as to the N_3 (particles with diameter larger than 3 nm) and N_{50} number concentrations. Concentrations of N_3 and N_{50} were consistently underestimated, while the best model performance (based on the Taylor model skill score) was achieved when the ELVOC yield from precursor VOCs was around 13%. These studies suggest that the role of organics and especially ELVOCs on particle formation and growth is still not well understood.

In this study we extend the three-dimensional regional chemical transport model (CTM), PMCAMx-UF (Jung et al., 2010), with detailed aerosol microphysics (Gaydos et al., 2007; Karydis et al., 2007) that has been used and evaluated for simulations over the US and Europe (Fountoukis et al., 2012). The number concentrations of particles with diameter larger than 10 nm (N_{10}) and 100 nm (N_{100}) were used for the analysis of the model predictions of Fountoukis et al. (2012), whereas Gordon et al. (2016) relied on N_3 and N_{50}. The N_3 and N_{10} are connected to some extent, but usually there are more reliable measurements available in more sites for N_{10}. The same applies for the N_{50} and N_{100} pair, but the N_{100} is often closer to the CCN sizes at moderate cloud supersaturations. N_{10} and N_{100} were chosen as the metrics in this study for continuity, given that they have been used in previous PMCAMx-UF evaluations.

Originally PMCAMx-UF assumed that growth of new particles was exclusively due to sulfuric acid and ammonia condensation while the semi-volatile secondary organics condensed only on the accumulation mode thus contributing to the condensation and coagulation sinks. This initial model version was found to reproduce more than 70% of the hourly number concentrations of N_{10} within a factor of 2 (Fountoukis et al., 2012). However, the concentration of N_{100} as proxy for the number of particles that can act as CCN) was systematically underpredicted. The growth rates were also underpredicted, with smaller errors in sites where the sulfate to organics mass ratio was high. These problems were caused mainly by insufficient organic vapor condensation (Fountoukis et al., 2012) on ultrafine particles. Patoulias et al. (2018) developed an extended version of PMCAMx-UF in which the SOA components were modeled as semi-volatile first-generation products of the oxidation of VOCs. The model predictions were compared against size distribution measurements from 16 stations in Europe during a photochemically active period.

123 Including SOA condensation on ultrafines in PMCAMx-UF improved its ability to reproduce the
124 N_{10} and N_{100} concentration at ground level. The inclusion of SOA decreased the daily normalized
125 mean bias (NMB) of N_{10} from 85% to 75% and the daily NMB of N_{100} from 40% to 20%. However,
126 the results suggested that there is a need for additional improvements.

127   The primary goal of this study is to examine the role of IVOCs and ELVOCs on particle
128 number concentrations in Europe. PMCAMx-UF is extended to simulate the multiple generations
129 of IVOC gas-phase oxidation and the production of ELVOCs by monoterpenes. This extended
130 version is used for the base case simulations in this study. The model predictions are compared
131 with measurements from 26 sites during the intensive field campaign that took place in Europe, as
132 part of the Pan-European-Gas-AeroSOl-climate-interaction Study (PEGASOS) project, from June
133 5 to July 8, 2012. The airborne data obtained by a Zeppelin measuring above Po-Valley during the
134 same campaign are also used. An analysis of the Zeppelin measurement can be found in Lampilahti
135 et al. (2021). Additional simulations are performed neglecting certain processes (e.g., production
136 of ELVOCs) to quantify their role in the model predictions.

137

138 **2. Model description**

139   PMCAMx-UF is a three-dimensional chemical transport model (CTM) that simulates the
140 aerosol number size distribution in addition to the mass/composition size distribution (Jung et al.,
141 2010; Fountoukis et al., 2012) and is described in detail in Patoulias et al. (2018). PMCAMx-UF
142 is based on the framework of PMCAMx (Gaydos et al., 2007; Karydis et al., 2007), describing the
143 processes of horizontal and vertical advection, emissions, horizontal and vertical dispersion, wet
144 and dry deposition, aqueous and aerosol phase chemistry, as well as aerosol dynamics and
145 thermodynamics.

146   For the simulation of aerosol microphysics, PMCAMx-UF uses the updated version of
147 DMANx which simulates the processes of coagulation, condensation/evaporation and nucleation
148 (Patoulias et al., 2015) with the two-moment aerosol sectional (TOMAS) algorithm (Adams and
149 Seinfeld, 2002; Jung et al., 2006). A key feature of TOMAS is its ability to track two independent
150 moments of the aerosol size distribution for each size bin: the aerosol number and mass
151 concentration.

152   The aerosol size distribution is discretized into 41 sections covering the diameter range from
153 approximately 0.8 nm to 10 μm. The lowest boundary is at 3.75×10^{-25} kg of dry aerosol mass per

154   particle. Each successive boundary has twice the mass of the previous one. The particle

155   components modeled include sulfate, ammonium, nitrate, sodium, chloride, crustal material,

156   water, elemental carbon, primary organic aerosol (POA) and eight surrogate SOA components.

157   In this work, the nucleation rate is calculated using a scaled ternary parameterization based

158   on the original expressions of Napari et al. (2002) with a scaling factor of 10^{-6} following the

159   suggestions of Fountoukis et al. (2012). The binary parameterization of Vehkamäki et al. (2002)

160   is employed if the NH_3 concentration is below a threshold value of 0.01 ppt.

161   Coagulation of particles in the atmosphere is an important sink of aerosol number but is

162   also a mechanism by which freshly nucleated particles grow to larger sizes. Following Adams and

163   Seinfeld (2002), TOMAS assumes that the aerosol particles coagulate via Brownian diffusion and

164   that the effects of gravitational settling and turbulence on coagulation are negligible. The

165   calculation of the coagulation coefficients is based on the wet diameters of the particles. These wet

166   diameters are calculated following the approach of Gaydos et al. (2005). For small particles (<100

167   nm), we use the expression of Dahneke et al. (1983) to correct for non-continuum effects. The

168   coagulation algorithm uses an adaptive time step. The time step is limited so that the aerosol

169   number or mass concentration in any size category does not increase by more than an order of

170   magnitude or decrease by more than 25% in each step.

171   The extended SAPRC (Statewide Air Pollution Research Center) chemical mechanism

172   (Carter, 2000; Environ, 2003), which includes 219 reactions of 64 gases and 18 free radicals, is

173   used for the gas phase chemistry mechanism in PMCAMx-UF. The SAPRC version used for this

174   work includes five lumped alkanes (ALK1-5), two lumped olefins (OLE1-2), two lumped

175   aromatics (ARO1-2), isoprene (ISOP), a lumped monoterpene (TERP) and a lumped sesquiterpene

176   species (SESQ).

177   Condensation of gas-phase species to existing aerosol particles is an important source of

178   aerosol mass and a means by which small particles grow to CCN sizes. Sulfuric acid is assumed

179   to be in pseudo-steady state in PMCAMx-UF. This pseudo steady-state approximation (PSSA) for

180   sulfuric acid proposed by Pierce and Adams (2009) increases the computational speed with a small

181   loss in accuracy. Jung et al. (2010) evaluated the performance of PSSA for sulfuric acid in DMAN

182   against a 4th order Runge-Kutta algorithm and showed that PSSA was accurate and

183   computationally efficient. Condensation of ammonia is simulated following the approach

184   described by Jung et al. (2006). Ammonia condensation on the ultrafine particles ends when sulfate

185   is fully neutralized to ammonium sulfate.

186   Nitric and hydrochloric acids partition to particles (as nitrate and chloride, respectively) in

187   the accumulation mode range in PMCAMx-UF assuming that the system is always in equilibrium.

188   The amounts of nitric acid and hydrochloric acid transferred at each time step between the gas and

189   aerosol phases are determined by applying the aerosol thermodynamic model ISORROPIA (Nenes

190   et al., 1998). This amount is then distributed over the aerosol size sections by using weighting

191   factors based on their effective surface area (Pandis et al., 1993).

192   PMCAMx-UF assumes that organics and inorganics are in different phases in the same

193   particles. Therefore, the condensation of one affects the size distribution of the particles and

194   therefore the condensation rate of the other. The inorganic aerosol thermodynamics including the

195   sulfate/bisulfate split and the water uptake by all inorganic aerosol components are simulated by

196   ISORROPIA. The water content of the organic aerosol is neglected in this version of PMCAMx-

197   UF and the aerosol water is dominated by the inorganic aerosol components. Additional

198   information can be found in previous publications describing the evolution of PMCAMx-UF (Jung

199   et al. 2010; Fountoukis et al. 2012; Patoulias et al. 2018).

200

2.1   Secondary organic aerosol formation

202   Gas-phase oxidation of VOCs produces semi-volatile and low-volatility products that can

203   then condense to the particle phase. The volatility-basis set (VBS) framework used in PMCAMx-

204   UF (Donahue et al., 2006) describes the volatility distribution of the OA compounds. SOA is

205   formed from anthropogenic (aSOA) and biogenic (bSOA) precursors. Each of these types is

206   simulated with 5 volatility bins with saturation concentrations of 10^{-5}, 1, 10, 100 and 1000 µg

207   m^{-3}. The 10^{-5} µg m^{-3} bin was added in this work to describe the ELVOCs. We assumed an average

208   molecular weight of 200 g mol^{-1} for SOA, and an effective enthalpy of vaporization of 30 kJ

209   mol^{-1} (Pathak et al., 2007; Stanier et al., 2007). The SOA yields used in this version of PMCAMx-

210   UF for the semi-volatile components are the NO_x-dependent stoichiometric yields of Murphy et

211   al. (2009).

212   Chemical reactions that change the volatility of the organics in the gas phase will change

213   the OA mass by influencing their partitioning. In PMCAMx-UF all secondary species are treated

214   as chemically reactive. Further gas-phase oxidation of OA vapors (chemical aging) is modeled

215 using a second-order reaction with hydroxyl radicals and a rate constant equal to 1×10^{-11} cm^3

216 molecule^{-1} s^{-1} (Atkinson and Arey, 2003). Each reaction is assumed to reduce the volatility of the

217 vapor material by one order of magnitude (i.e., shifting material from a C* of 100 to 10 μg m^{-3}),

218 with a small increase in mass (7.5%) to account for the added oxygen (Lane et al., 2008;

219 Shrivastava et al., 2008). IVOCs were not included in the original emission inventory and therefore

220 have been added to the emissions. The IVOC emission rate is estimated based on the non-volatile

221 POA emissions included in the inventory and is assumed to be 1.5 times the non-volatile POA

222 emissions. IVOCs are distributed in the 10^3, 10^4, 10^5, and 10^6 μg m^{-3} saturation concentration bins

223 and their emission rates are assumed to be equal to 0.3, 0.4, 0.5 and 0.8 times the original non-

224 volatile POA emission rate, for the 10^3-10^6 bins respectively (Robinson et. 2007).

225   ELVOCs were assumed to be produced by the oxidation of monoterpenes with a molar

226 yield of 5%. For comparison, ELVOCs yields for the α-pinene ozonolysis in Jokinen et al. (2015)

227 were 3.4 ± 1.7%, by Ehn et al. (2014) of 7 ± 4% and 4.5 ± 3.8% in Rissanen et al. (2014). An

228 average molecular weight of 200 g mol^{-1} for ELVOCs was assumed in this work.

229   The partitioning of OA between the gas and particulate phases is simulated dynamically in

230 PMCAMx-UF without assuming equilibrium (Patoulias et al., 2015). The driving force for

231 condensation of a vapor to an aerosol particle is the difference between its ambient vapor partial

232 pressure and the equilibrium vapor pressure over the particles, with the latter including the Kelvin

233 effect which is due to the curvature of the particles. The Kelvin effect is larger for the smaller

234 particles and acts as a barrier for the condensation of organic vapors on these particles. In this

235 simulation a surface tension of σ=0.025 N m^{-1} is assumed for all SOA components (Pierce et al.,

236 2011; Patoulias et al. 2015).

237   Three different chemical schemes are used in this work (Table 1). The first scheme (case

238 1 or base case) includes (i) the aging of SOA components from anthropogenic sources, using a rate

239 constant k (298 K) = 10×10^{-12} cm^3 molecule^{-1} s^{-1} (anthropogenic SOA aging), (ii) the aging of

240 IVOCs using a rate constant k (298 K) = 40×10^{-12} cm^3 molecule^{-1} s^{-1}, (iii) production of ELVOCs

241 with saturation concentration of 10^{-5} μg m^{-3} from the oxidation of monoterpenes with a yield of

242 5%. The aSOA aging rate constant is based on OH oxidation of the products of aromatic VOCs

243 oxidation (Atkinson 2000; 2003). No biogenic SOA aging was simulated in this case, an

244 assumption based on laboratory studies (Presto et al., 2006; Ng et al., 2006) and the results of Lane

245 et al. (2008). In the second simulation (case 2), the ELVOC yield was set to zero thus neglecting

246 their formation. The rest of the parameters were the same as in the base case. Finally, in the third

247 simulation the emissions of IVOCs and the chemical aging reactions of all VOCs were neglected

248 while the production of the ELVOCs was simulated similarly to the base case.

249

250 **2.2 Model application and measurements**

251 The PMCAMx-UF modeling domain in this application covers a 5400×5832 km^2 region

252 in Europe, with a 36×36 km grid resolution and 14 vertical layers extending up to approximately

253 7.2 km. The modeling period covers 34 days, from June 5 to July 8, 2012 corresponding to the

254 PEGASOS 2012 intensive period. PMCAMx-UF was set to perform simulations on a rotated polar

255 stereographic map projection. The first two days of each simulation were excluded from the

256 analysis to minimize the effect of the initial conditions on the results. For the boundary conditions,

257 constant and relatively low values have been used (Table S1) so that the predicted particle number

258 concentrations over central Europe are determined for all practical purposes by the emissions and

259 corresponding processes simulated by the model. The boundary conditions are identical to those

260 used in Patoulias et al. (2018). The effect of these boundary conditions on the predicted number

261 concentrations are discussed in Patoulias et al. (2018).

262 Meteorological inputs to PMCAMx-UF include horizontal wind components, vertical

263 diffusivity, temperature, pressure, water vapor, clouds, and rainfall. The Weather Research and

264 Forecasting (WRF) model (Skamarock et al., 2005) was used to generate the above inputs. WRF

265 was driven by geographical and dynamic meteorological data generated by the Global Forecast

266 System (GFSv15) of the National Oceanic and Atmospheric Administration/National Centers for

267 Environmental Prediction. Each layer of PMCAMx-UF was aligned with the layers used in WRF.

268 The WRF simulation was periodically re-initialized every 3 days with observed conditions to

269 ensure accuracy in the corresponding fields used as inputs in PMCAMx-UF. The measurements

270 were pre-processed by the WPS (WRF Preprocessing System) package, which provides each

271 atmospheric and static field with fidelity appropriate to the chosen grid resolution of the model.

272 The performance of WRF for Europe against observed meteorological variables has been the topic

273 of several recent studies (Jimenez-Guerrero et al., 2008; de Meij et al., 2009; Im et al., 2010;

274 Argueso et al., 2011; Garcia-Diez et al., 2012) demonstrating good performance.

275 The particle emissions were based on the pan-European anthropogenic particle number

276 emission inventory (Denier van der Gon et al., 2009; Kulmala et al., 2011) and the carbonaceous

aerosol inventory (Kulmala et al., 2011) developed during the EUCAARI (European Integrated project on Aerosol, Cloud, Climate, and Air Quality Interactions) project. The resulting number/mass inventories includes both number emissions and consistent size-resolved composition for particles over the size range of approximately 10 nm to 10 μm. Hourly gridded anthropogenic and biogenic emissions included both gases and primary particulate matter. The natural emissions include both particulate matter and gases and combine three different data sets: emissions from ecosystems based on the Model of Emissions of Gases and Aerosols from Nature (MEGAN; Guenther et al., 2006), marine emissions based on the model of O'Dowd et al. (2008) as sea surface covers a considerable area of the domain, and wildfire emissions (Sofiev et al., 2008a, b). MEGAN uses as inputs the plant functional type, the leaf area index, various chemical species emission factors and weather data provided by the WRF. Wind speed fields from WRF and chlorophyll-a concentrations were used as inputs of the marine aerosol model. VOCs were speciated based on the approach proposed by Visschedijk et al. (2007). Anthropogenic gas emissions included land emissions from the GEMS (global and regional Earth-system monitoring using satellite and in-situ data) dataset (Visschedijk et al., 2007). The international shipping, industrial, domestic, agricultural and traffic aerosol emission sources were included in the anthropogenic inventory (Denier van der Gon et al., 2009; Kulmala et al., 2011).

The model results were compared against measurements in 26 ground sites, which are available in the European Supersites for Atmospheric Aerosol Research (EUSAAR), and EBAS databases (https://ebas.nilu.no) and the Aerosols, Clouds and Trace gases Research Infrastructure (ACTRIS) (https://actris.nilu.no). Particle size distribution measurements at all sites were made using either a Differential Mobility Particle Sizer (DMPS) or a Scanning Mobility Particle Sizer (SMPS). Information about all stations can be found in Table S2.

An intensive field campaign took place in Europe, as part of the Pan-European-Gas-AeroSOl-climate-interaction Study (PEGASOS) project, from June 5 to July 8, 2012. Measurements of aerosol mass concentration PM_1 (particulate matter particles of diameter less than 1 micrometer) from the PEGASOS project are also available for the same period for Patras (Greece), Finokalia (Greece), San Pietro Capofiume (Italy) and Bologna (Italy) (Table S3a) and filter $PM_{2.5}$ (particulate matter particles of diameter less than 2.5 micrometer) measurements from 6 additional stations in Europe (Table S3b). The organic aerosol mass concentration was estimated

307   from the organic carbon measurements assuming an organic mass to carbon ratio equal to 1.8

308   (Kostenidou et al., 2015).

309   The measurement of organic carbon and therefore the estimated OA using filters is

310   characterized by two main artifacts: a positive one involving adsorption of organic vapors on the

311   quartz filters used for the sampling and a negative one related to the evaporation of some of the

312   semi-volatile material (Turpin et al., 2000; Mikuška et al., 2011). There is a rich literature on the

313   magnitude of these artifacts and on ways to minimize them or correct for them (involving denuders

314   for removal of organic vapors and after-filters). In this work, we use the reported measurements

315   for the model evaluation keeping in mind their uncertainty.

316   The airborne measurements acquired by the PEGASOS Zeppelin were acquired during the

317   simulation period over the Po Valley. The Po Valley region is situated between the Alps in the

318   north and the Apennines Mountains in the south–southwest. The mountains surround the valley on

319   three sides and high levels of pollutants are often observed in the region due to the industrial,

320   agricultural, and other anthropogenic emissions. In addition, emissions from ship traffic on the

321   Adriatic Sea (Hamed et al., 2007) and long-range transport from central-eastern Europe also

322   contribute pollutants to the region (Sogacheva et al., 2007). A SMPS was used to measure the

323   number size distribution of particles in the size range of 10 to 430 nm. Details of the relevant

324   PEGASOS Zeppelin measurements can be found in Lampilahti et al. (2021).

325

326   **3. Results**

327   **3.1   Base case**

328   The average predicted ground level average number concentrations for the total number of

329   particles (N_{tot}) and for particles with diameters above 10 nm (N_{10}), 50 nm (N_{50}) and 100 nm (N_{100}),

330   during June 5 to July 8, 2012 are shown in Figure 1. The N_{50} and N_{100} concentrations are often

331   used as proxies for CCN number concentrations (Fountoukis et al., 2012). On a domain average

332   basis, the model predicted for the ground level 4780 cm^{-3} for N_{tot}, 3630 cm^{-3} for N_{10}, 1990 cm^{-3}

333   for N_{50}, and 820 cm^{-3} for N_{100} during the simulated period. The highest N_{tot} average concentrations

334   (more than 15000 cm^{-3}) were predicted over Bulgaria, southern Romania, Turkey, Poland,

335   Holland, Portugal, Northern Spain, Eastern UK and Russia. On the other hand, the highest N_{50} and

336   N_{100} are predicted over the Mediterranean, mainly in areas near Southern Spain, Southern Italy,

337   and the Balkans. The N_{tot} and N_{10} are high in areas of frequent nucleation events and areas with

338 high particle number emissions, whereas the N_{50} and N_{100} levels are affected significantly by

339 secondary particulate matter production. The high photochemical activity over the Eastern

340 Mediterranean leads to the corresponding high levels of N_{50} and N_{100} during this period.

341

3.2 Evaluation of PMCAMx-UF predictions

3.2.1 Comparison of PMCAMx-UF predictions to ground aerosol number observations

344   The prediction skill metrics of PMCAMx-UF, for the daily average ground measurements

345 from the 26 stations, are summarized in Tables 2 and 3 for both the base case and the case in which

346 the ELVOCs are neglected.

347   For the base case simulation, the model has a tendency to overestimate the N_{10} levels. The

348 normalized mean bias (NMB) for the daily average concentrations is 23% and the normalized

349 mean error (NME) 63%. The N_{10} was overpredicted in 18 sites, underpredicted in 7 and there was

350 practically zero bias (less than 0.1%) in the last station. The NMB in 8 sites (Prague-Suchdol,

351 Ispra, Melpitz, Patras, K-Puszta, Hohenpeissenberg, Hyytiälä and San Pietro Capofiume) was less

352 than ±15%, and for another 8 stations between ±15% and ±40% (Annaberg-Buchholz, Cabauw,

353 Dresden Nord and Winckelmannstrasse, Finokalia, Giordan Lighthouse, Kosetice, Montseny and

354 Varrio). The highest discrepancies with the measurements of N_{10} were found in Aspvreten,

355 Birkness II, Usti n.L.-mesto, Vavihill, Vielsalm, Zugspitze-Schneefernerhaus, Waldhof, Costa

356 Navarino, and Thesssaloniki with NMB higher than ±40%.

357   The model performed better for N_{100}. There was little bias in the corresponding predictions

358 on average (the NMB was -10%) and the NME was 45%. The NMB for 10 sites (Cabauw, Giordan

359 Lighthouse, Hyytiälä, Kosetice, Melpitz, Patras, Prague-Suchdol, Vielsalm, Waldhof and

360 Zugspitze) was less than ±15% and for another 12 (Annaberg-Buchholz, Birkenes II, Dresden

361 Nord and Winckelmannstrasse, Finokalia, Hohenpeissenberg, Ispra, K-Puszta, Montseny, Costa

362 Navarino, San Pietro Capofiume, Usti n.L-mesto. and Vavihill) between ±15% and ±40% (Table

363 3). The absolute NMB for N_{100} exceeded 40% only in Aspvreten, Varrio and Thessaloniki.

3.3.2 Evaluation of aerosol composition predictions

365   The PMCAMx-UF predictions can be evaluated during that period using available PM_1

366 measurements from Aerosol Mass Spectrometers at four stations (Bologna and San Pietro

367 Capofiume, in Italy and Finokalia and Patras, in Greece) that were part of the PEGASOS

368 campaign.

369   In Italy and Greece, the model reproduces the observations of the PM_1 concentrations of

370   the major inorganic aerosol components (sulfate, ammonium, nitrate) reasonably well (Table 4).

371   The model tends to underpredict the organic aerosol concentrations in Patras and Bologna, while

372   it overpredicts the OA in Finokalia and San Pietro Capofiume (Table 5). The OA NMB is -2% and

373   the NME is 38%, with the Finokalia site presenting the higher NMB value (50%) and San Pietro

374   Capofiume, Bologna the lower (±20%) (Table 5).

375   For the rest of Europe, $PM_{2.5}$ filter measurements have been used, available in the European

376   Supersites for Atmospheric Aerosol Research (EUSAAR) and EBAS databases

377   (http://ebas.nilu.no/) for stations that had available data for more than 15 days during the simulated

378   period (6 additional stations in Europe: Payerne, Melpitz, Montseny, Ispra, Diabla Gora, and

379   Iskrba; Table 6). For the calculation of OA mass concentration, we assumed OA:OC=1.8

380   (Kostenidou et al., 2015). For these sites, the model has a tendency towards overestimating the

381    $PM_{2.5}$ OA concentration for 4 out of 6 stations, presenting an average NMB of 20% and NME of

382   62% (Table 6).

383 3.3.3 Comparison of PMCAMx-UF predictions to Zeppelin measurements

384   One of the challenges of the PMCAMx-UF evaluation using airborne measurements is that

385   the model predictions are available every 15 min while the corresponding measurements by the

386   Zeppelin were taken every 3 min in different heights. For comparison purposes, the model output

387   was interpolated to the times of the Zeppelin measurement periods. PMCAMx-UF reproduced

388   more than 75% of the 2000 3-min N_{10} and N_{100} measurements by the Zeppelin with a factor of 2

389   (Figure S1). The vertical profiles shown in Fig.2, are averages of different flights that collected

390   data in different days and different altitudes each time. The number of samples at different altitudes

391   changed for each flight creating additional variability in the measured profiles.

392   To facilitate the comparison between measurements and predictions the corresponding

393   average profiles (matched in space and time) were calculated using 80 m altitude bins for all the

394   PEGASOS flights. PMCAMx-UF reproduced on average the N_{10} measurements over Po Valley at

395   the lower 160 m and above 400 m but underestimated the higher N_{10} levels measured in the residual

396   layer at heights between 160-400 m at several of the flights that started several hours before sunrise

397   (Fig. 2a). The average measured N_{10} at all heights was 6,000 cm^{-3}, while the predicted

398   concentration was equal to 4,700 cm^{-3}. PMCAMx-UF reproduced well the N_{100} concentration at

399   all heights (Fig 2b). The model also reproduced 80% of the 3-min N_{100} Zeppelin measurements

within a factor of 2. The measured average N_{100} at all heights was 1,500 cm^{-3} and the average predicted by PMCAMx-UF was 1,800 cm^{-3}. The ability of the revised model to reproduce reasonably well the high-time resolution (3-minute) Zeppelin measurements at multiple altitudes and locations is encouraging. The predictions of PMCAMx-UF for the aerosol mass concentration were compared to the Zeppelin PM$_1$ composition measurements obtained by an AMS (each 3 minutes, 9 flights, ~1300 data points). The average vertical profiles of organics, sulfate, ammonium, and nitrate are shown in Fig. S2. Overall, the model performance aloft was quite similar with that at the ground level. For example, for the 9 Zeppelin flights the OA normalized mean bias was -4% and the normalized mean error equal to 40% (Table S4). The measured and the predicted OA mean values are 4.6 and 4.4 μg m^{-3}, respectively.

3.2   Effect of ELVOC production on particle number and OA concentrations

An additional simulation was performed neglecting the production of ELVOCs from terpenes (case 2). The addition of ELVOCs, increased the PM$_{2.5}$ OA mass by approximately as much as 0.5 μg m^{-3} in Central/Eastern Europe and Russia, accounting for approximately 10-15% of the OA (Fig. 3). In these areas a combination of high terpene emissions and high photochemical reaction rates existed during the simulated period. The highest relative predicted increase of OA was 15-25% in northern Europe. In central Europe the ELVOC formation increased average OA by approximately 10%.

The average fractional increase of N_x, due to the production of ELVOCs is calculated as:

$$f_{Nx} = \frac{N_x(with\ ELVOCs) - N_x(without\ ELVOCs)}{N_x(without\ ELVOCs)} \tag{1}$$

where, x, is 10, 50, 100 nm or zero (total number). Rather surprisingly, the average fractional change for all number concentrations (N_{tot}, N_{10}, N_{50} and N_{100},) is small ranging between 1% and -4% (Fig. 4) (N_{tot}: -8 cm^{-3} or -0.14%, N_{10}: 40 cm^{-3} or -1.14%, N_{50}: 60 cm^{-3} or 3 %, N_{100}: 35 cm^{-3} or 4%). One reason for the small average change is that both increases and decreases are predicted for different areas in Europe. These mixed results are due to the fact that the ELVOC condensation accelerates the growth of new and preexisting particles to larger sizes, but at the same time accelerates their losses due to the increase of the coagulation sink and decreases the nucleation rate due to the increase of the condensation sink.

The formation of ELVOCs resulted in a predicted decrease of N_{tot} by 20% (300-600 cm^{-3}) in parts of the Nordic countries and by 5% in central Europe (Fig. 4). The decreases are predicted

431   for most Europe with the exception of a few areas in which increases are predicted (northern

432   Iberian Peninsula, parts of France, areas in the Balkans with high sulfur dioxide levels, etc.) (Fig.

433   5). The predicted N_{10} increased by 5-15% (150-400 cm^{-3}) over Finland, northwestern Russia,

434   France, Ireland and northern Portugal. At the same time there were small decreases of a few percent

435   over several areas in Europe especially in the south and in the east as well over the Baltic Sea. N_{50}

436   increased over almost of Europe by 50 to 300 cm^{-3}. This N_{50} increase corresponds to 20-40% over

437   Scandinavia and northwestern Russia, and 10% for central Europe. Finally, the ELVOCs caused

438   an increase in N_{100} of 20-50% over Scandinavia and 10-20% increases over central Europe. The

439   absolute corresponding N_{100} changes in these areas are 100-200 cm^{-3}.

440   The corresponding changes of the number concentrations for particles with diameters

441   between 1 and 10 nm (N$_{1–10}$), 10 and 50 nm (N$_{10–50}$) and (iii) 50 and 100 nm ($N_{50–100}$) are

442   summarized in Fig. S3. These figures illustrate the complex effect of the ELVOCs on different

443   parts of the aerosol number distribution. Decreases in the concentrations of the 1-10 nm particles

444   (decreasing nucleation rate due to increased condensation sink, increasing coagulation with larger

445   particles), increases in the concentrations of the particles with diameter larger than 100 nm (due to

446   accelerated growth of the sub-100 nm particles to larger sizes) and both increases and decreases in

447   the 10-50 nm size range depending on the magnitude of the different competing processes in each

448   area. The effect of the ELVOCs in this PMCAMx simulation is clearly a lot more complex than a

449   uniform increase of particle number concentrations.

450   The spatial variability of the fractional change in the number concentration of N_{1-10}

451   (reflecting nucleation rates), sulfuric acid concentration, condensational sink (CS) and coagulation

452   sink due to the ELVOCs is depicted in Figure S4. In areas such as the Scandinavian Peninsula the

453   production of ELVOCs is predicted to lead to a 20-30% average increase of the coagulation and

454   condensational sinks and a corresponding decrease of sulfuric acid levels and N_{1-10}. Similar

455   changes are predicted for several other areas (e.g., Central Europe) but are less pronounced.

456   The results in the Hyytiälä station in Finland were examined in more detail because the

457   predicted number concentrations in Finland are quite sensitive, according to PMCAMx-UF, to the

458   addition of the ELVOCs. The predicted N_3, N_{10}, N_{50} and N_{100} concentrations for the base case are

459   in reasonable agreement with the field measurements in this area (Figure S5), with a tendency of

460   the model to overpredict the N_3 levels during a few nucleation events. For all concentrations the

461   simulation with the ELVOCs (base case) reproduces the measurements better than the simulation

in which they are neglected. The condensation sink for Hyytiälä increases by a few percent due to the additional mass of the ELVOCs (Figure S5). The average measured and predicted number size distributions in Hyytiälä are shown in Figure S6. The addition of the ELVOCs leads to increased levels in the part of the size distribution above 50 nm. A decrease of the concentration of particles with diameter below 7 nm is predicted due to the addition of the ELVOCs because of both increased coagulation losses but also lower nucleation rates. The difference in the predictions of the two simulations (with and without ELVOCs) in Hyytiälä is modest. The discrepancy between model predictions and measurements is due to both weaknesses of the measurements (particles smaller than 3 nm were not measured) and a tendency of the model to overpredict nucleation event intensity in this area.

The ELVOC addition played a minor role on the overall performance of PMCAMx-UF. The NMB for N_{10} decreased (in absolute terms) by 1%, it increased by 5% for N_{100} due to the addition of the ELVOCs in the simulation (Table 2-3). The addition of the ELVOCs affects mainly the PMCAMx-UF predictions in northern Europe and especially Finland, where the predictions of N_{100} significantly improve. In Hyytiälä the NMB decreases from -34% to -14% and in Varrio drops from -72% to -49% (Table 3). The corresponding normalized mean errors changed by 1-2%. These small changes in the performance metrics are consistent with the small overall changes caused by the ELVOC addition.

The small change in the OA mass concentration due to the addition of the ELVOCs has a modest impact on the performance of PMCAMx-UF for OA (Table S5 and S6). For example, the PM_1 OA bias improves from -6% to 2% while the $PM_{2.5}$ OA bias increases from 15% to 20%. The changes in normalized error are 1% or less.

3.3 Effect of IVOCs on particle number concentrations

The emissions of IVOCs ($C^* \geq 10^{-3}$ μg m^{-3}) were set to zero in a sensitivity test (Case 3) to quantify their effect on the predicted particle number concentration and size distribution. The SOA formed by the IVOCs (SOA-iv) exceeds 1 μg m^3 in southern Europe, over the Mediterranean Sea, but also in large areas over central and eastern Europe (Fig. 6). The high SOA-iv levels over the Mediterranean are due to the oxidation of IVOCs emitted from large wildfires that occurred during the simulation period. The corresponding SOA-iv is 10-25% of the total OA over

492 continental Europe and even higher (about 60%) over parts of the marine atmosphere. The average

493 fractional increase of N_x, due to emission and aging of IVOCs is calculated as:

494 $$f_{Nx} = \frac{N_x(with\ IVOCs) - N_x(without\ IVOCs)}{N_x(without\ IVOCs)} \tag{2}$$

495 where, x, is 10, 50, 100 nm or zero (total number).

496 According to PMCAMx-UF the addition of the emissions of IVOCs and their aging

497 reactions lead to a reduction of N_{tot} by 5-10% and N_{10} by 5% (Fig. 7) for continental Europe. On

498 the other hand, this addition of IVOCs leads to an increase of N_{50} by 5% and N_{100} by 5-10% mainly

499 in central Europe and the Mediterranean Sea (Fig. 7). The corresponding changes of the number

500 concentrations for the various size ranges N_{1-10}, N_{10-50} and N_{50-100} are summarized in Fig. 8. The

501 predicted N_{1-10} decreases approximately 15-20% for most of Europe except for the Scandinavian

502 peninsula due to the IVOCs. N_{10-50} decreases 10-15% mainly in southern Europe and N_{50-100}

503 changes less than ±5% or ±100 cm^{-3} in the simulated domain.

504 The atmospheric oxidation of the emitted IVOCs produces semi-volatile organic

505 compounds, which condense preferentially on particles in the accumulation mode and not so much

506 on the smallest particles due to the Kelvin effect. This results in an increase of both the

507 condensation and coagulation sinks, which then lead to a decrease of the nucleation rate but also

508 on the coagulation rate of the smaller with the larger particles.

509 The effect of the addition of the IVOCs on the performance of PMCAMx-UF is modest and

510 mixed. The NMB for N_{10} increased by 4% (from 23% to 27%) and decreased by 5% for N_{100} (from

511 10% to 5%) (Table S7). The corresponding NME for both N_{10} and N_{100} changed slightly

512 (approximately 1%). The modest overall changes on the number distribution of the ultrafine

513 particles caused by the addition of IVOCs and the corresponding aging reactions are consistent

514 with the small changes in the PMCAMx-UF performance metrics.

515 The addition of the IVOCs and the resulting SOA-iv from their oxidation also had mixed

516 results in the PMCAMx-UF performance for OA in Europe. This added SOA removed the

517 underprediction of OA against the AMS measurements in Italy and Greece; the NMB changed

518 from -18% when IVOCs were neglected to 2% when IVOCs were included (Table S8). The NME

519 decreased a little (from 38% to 35%) with the IVOC addition. The performance against the OA

520 measurements in the other European sites became a little worse when IVOCs were included in the

521 model (Table S9). The small underprediction (NMB=-8%) in OA became a larger overprediction

522 (NMB=20%) and the NME increased from 50% to 62%. These results are characteristic of the

523   uncertainties in primary OA emissions but also SOA production from the various VOCs and
524   IVOCs emitted by anthropogenic and biogenic sources.

525

526   **4. Conclusions**

527   A new version of PMCAMx-UF was developed with the ability to simulate the formation
528   and dynamic condensation of ELVOCs during the oxidation of the monoterpenes and the
529   emissions and multi-generational chemistry of IVOCs. The model was applied to the PEGASOS
530   summer intensive period campaign during the summer of 2012. The available measurements
531   included both ground stations across Europe and airborne measurements from a Zeppelin over the
532   Po Valley.

533   The number concentration predictions of PMCAMx-UF, are compared against ground
534   measurements from 26 stations in Europe. The model tends to overestimate daily average N_{10} with
535   a normalized bias of 35% and an average error of 64%. PMCAMx-UF performed well for N_{100}
536   with a low bias (-2 %) and an error of 41%. The performance of the model in the lowest 1 km of
537   the atmosphere above Po Valley for both N_{10} and N_{100} was even better than its average performance
538   over Europe. The model's predicted PM_1 and $PM_{2.5}$ concentrations and composition had NMB of
539   15% and errors less than 60% depending on the PM component. These results suggest that
540   PMCAMx-UF does a reasonable job reproducing the aerosol mass and number concentrations over
541   Europe during the simulated period.

542   The ELVOCs produced by the monoterpene oxidation contributed, according to the
543   PMCAMx-UF predictions on average around 0.5 μg m^{-3} and accounted for 10-15% of the $PM_{2.5}$
544   OA. The highest relative predicted increase of OA was 15-25% in northern Europe, while the
545   ELVOC formation increased average OA by approximately 10% in central Europe.

546   The ELVOC production by monoterpenes led to surprisingly small changes of the average
547   number concentrations over Europe. The total number concentration decreased by 0.2%, the N_{10}
548   decreases by 1.1%, while N_{50} increased by 3% and N_{100} by 4% due to this new SOA source. One
549   of the reasons for these small average increases is the nonlinearity of the system leading to both
550   increases and decreases in different parts of Europe. Even if ELVOCs accelerate the growth of the
551   newly formed particles to larger sizes increasing in this way their lifetime, at the same time they
552   increase the aerosol mass and surface area as they mostly condense on the accumulation mode.
553   Therefore, they increase the condensation sink, decreasing the sulfuric acid supersaturation and

554 the corresponding nucleation rate. They also increase the coagulation sink and thus accelerate the

555 removal of all nanoparticles.

556 Locally the effects of the ELVOC production could be higher. For example, it is estimated

557 that the ELVOC productions leads to a decrease of the total particle concentration N_{tot} by 20% in

558 parts of the Nordic countries and by 5% in central Europe. At the same time, the predicted N_{10}

559 increased by 5-15% (150-400 cm^{-3}) over Finland, northwestern Russia, France, Ireland and

560 northern Portugal due to these secondary organic compounds. The predicted N_{50} increased almost

561 everywhere in continental Europe by 50-300 cm^{-3}. This is 10% increase of N_{50} over central Europe

562 and 20-40% over Scandinavia and northwestern Russia.

563 The addition of IVOC emissions and their aging reactions led to surprising reduction of the

564 total number of particles (N_{tot}) and N_{10} by 10-15 and 5-10%, respectively, and to an increase of the

565 concentration of N_{100} by 5-10%. In this case semi-volatile organic mass is produced, which

566 condenses preferentially on particles in the accumulation mode, increasing the condensation and

567 coagulation sinks and leading to a decrease in the concentration of the sub-10 nm particles.

568

569 **Data and code availability.** Field measurement data are available in ebas.nilu.no and

570 https://actris.nilu.no/. The Zeppelin-relevant, San Pietro Capofume and Bologna data are available

571 in https://doi.org/10.5281/zenodo.4660145 (Lampilahti et al. 2021). The field datasets for Patras,

572 Thessaloniki and Costa Navarino can be obtained after request to the authors. The PMCAMx-UF

573 is available from the authors (spyros@chemeng.upatras.gr).

574
575 **Supplement.**

576

577 **Author contributions.** DP wrote the code, conducted the simulations, analyzed the results, and

578 wrote the paper. SNP was responsible for the design of the study and the synthesis of the results

579 and contributed to the writing of the paper.

580

581 **Competing interests.** The authors declare that they have no conflict of interest.

582

References

Adams, P. J. and Seinfeld, J. H.: Predicting global aerosol size distributions in general circulation models, J. Geophys. Res., 107, 4370, https://doi.org/10.1029/2001JD001010, 2002.

Argueso, D., Hidalgo-Munoz, J. M., Gamiz-Fortis, S. R., and Esteban-Parra, M. J.: Evaluation of WRF parameterizations for climate studies over Southern Spain using a multistep regional-ization, J. Climate, 24, 5633–5651, 2011.

Atkinson, R.: Atmospheric chemistry of VOCs and NO_x, Atmos. Environ., 34, 2063–2101, 2000.

Atkinson, R. and Arey, J.: Atmospheric degradation of volatile organic compounds, Chem. Rev., 103, 4605–4638, doi:10.1021/cr0206420, 2003.

Carter, W. P. L.: Programs and files implementing the SAPRC-99 mechanism and its associates emissions processing procedures for Models-3 and other regional models, January 31, 2000.

Dahneke, B.: Simple Kinetic Theory of Brownian Diffusion in Va- pors and Aerosols, Theory of Dispersed Multiphase Flow, edited by Meyer, R. E., Academic Press, New York, 97–133 pp., 1983.

Dal Maso, M., Kulmala, M., Riipinen, I., Wagner, R., Hussein, T., Aalto, P., and Lehtinen, K. E. J.: Formation and growth of fresh atmospheric aerosols: eight years of aerosol size distribution data from SMEAR II, Hyytiälä, Finland, Boreal Environ. Res., 10, 323–336, 2005.

de Gouw, J. A., et al.: Budget of organic carbon in a polluted atmosphere: Results from the New England Air Quality Study in 2002, J. Geophys. Res., 110, D16305, doi:10.1029/ 2004JD005623, 2005.

de Meij, A., Gzella, A., Cuvelier, C., Thunis, P., Bessagnet, B., Vinuesa, J. F., Menut, L., and Kelder, H. M.: The im- pact of MM5 and WRF meteorology over complex terrain on CHIMERE model calculations, Atmos. Chem. Phys., 9, 6611– 6632, 2009.

Denier van der Gon, H. A. C., Visschedijk, A. J. H., Johansson, C., Hedberg Larsson, E., Harrison, R., and Beddows, D.: Size resolved pan European anthropogenic particle number inventory, EUCAARI Deliverable report D141 (available on request from EUCAARI project office), TNO, the Netherlands, 2009.

Docherty, K. S. et al.: Apportionment of Primary and Secondary Organic Aerosols in Southern California during the 2005 Study of Organic Aerosols in Riverside (SOAR-1), Environ. Sci. Technol., 42, 7655–7662, 2008.

Donahue, N. M., Robinson, A. L., Stanier, C. O., Pandis, S. N.: Coupled partitioning, dilution, and chemical aging of semivolatile organics, Environ. Sci. Technol., 40, 2635-2643, 2006.

Donahue, N. M., Epstein, S. A., Pandis, S. N., and Robinson, A. L.: A two-dimensional volatility basis set: 1. organic-aerosol mixing thermodynamics, Atmos. Chem. Phys., 11, 3303–3318, doi:10.5194/acp-11-3303-2011, 2011.

Dzepina, K., Volkamer, R. M., Madronich, S., Tulet, P., Ulbrich, I. M., Zhang, Q., Cappa, C. D., Ziemann, P. J., and Jimenez, J. L.: Evaluation of recently proposed secondary organic aerosol models for a case study in Mexico City, Atmos. Chem. Phys., 9, 5681-5709, 2009.

Ehn, M., Thornton, J. A., Kleist, E., Sipilä, M., Junninen, H., Pulli- nen, I., Springer, M., Rubach, F., Tillmann, R., Lee, B., Lopez- Hilfiker, F., Andres, S., Acir, I. H., Rissanen, M., Jokinen, T., Schobesberger, S., Kangasluoma, J., Kontkanen, J., Nieminen, T., Kurtén, T., Nielsen, L. B., Jørgensen, S., Kjaergaard, H. G., Canagaratna, M., Dal Maso, M., Berndt, T., Petäjä, T., Wahner, A., Kerminen, V. M., Kulmala, M., Worsnop, D. R., Wildt, J., and Mentel, T. F.: A large source of low-volatility secondary organic aerosol, Nature, 506, 476–479, 2014.

645   Environ, User's guide to the comprehensive air quality model with extensions (CAMx), version

646   4.02, report, ENVIRON Int. Corp., Novato, Calif, 2003.

647   Fanourgakis, G. S., Kanakidou, M., Nenes, A., Bauer, S. E., Bergman, T., Carslaw, K. S., Grini,

648   A., Hamilton, D. S., Johnson, J. S., Karydis, V. A., Kirkevåg, A., Kodros, J. K., Lohmann, U.,

649   Luo, G., Makkonen, R., Matsui, H., Neubauer, D., Pierce, J. R., Schmale, J., Stier, P.,

650   Tsigaridis, K., van Noije, T., Wang, H., Watson-Parris, D., Westervelt, D. M., Yang, Y.,

651   Yoshioka, M., Daskalakis, N., Decesari, S., Gysel-Beer, M., Kalivitis, N., Liu, X., Mahowald,

652   N. M., Myriokefalitakis, S., Schrödner, R., Sfakianaki, M., Tsimpidi, A. P., Wu, M., and Yu,

653   F.: Evaluation of global simulations of aerosol particle and cloud condensation nuclei number,

654   with implications for cloud droplet formation, Atmos. Chem. Phys., 19, 8591–8617, 2019.

655   Fountoukis, C., Riipinen, I., Denier Van Der Gon, H. A. C., Charalampidis, P. E., Pilinis, C.,

656   Wiedensohler, A., O'Dowd, C., Putaud, J. P., Moerman, M. and Pandis, S. N.: Simulating

657   ultrafine particle formation in Europe using a regional CTM: Contribution of primary

658   emissions versus secondary formation to aerosol number concentrations, Atmos. Chem. Phys.,

659   12, 8663–8677, 2012.

660   Garcia-Diez, M., Fernandez, J., Fita, L., and Yague, C.: Sea- sonal dependence of WRF model

661   biases and sensitivity to PBL schemes over Europe, Q. J. Roy. Meteor. Soc., 139, 501–514,

662   2012.

663   Gaydos, T. M., Stainer, C. O., and Pandis, S. N.: Modeling of in-situ ultrafine atmospheric particle

664   formation in the eastern United State, J. Geophys. Res., 110, D07S12, https://doi.org/10.1029/

665   2004JD004683, 2005.

666   Gaydos, T., Pinder, R., Koo, B., Fahey, K., Yarwood, G., and Pan- dis, S. N.: Development and

667   application of a three-dimensional Chemical Transport Model, PMCAMx, Atmos. Environ.,

668   41, 2594–2611, 2007.

669   Gordon, H., Sengupta, K., Rap, A., Duplissy, J., Frege, C., Williamson, C., Heinritzi, M., Simon,

670   M., Yan, C., Almeida, J., Tröstl, J., Nieminen, T., Ortega, I. K., Wagner, R., Dunne, E. M.,

671   Adamov, A., Amorim, A., Bernhammer, A.-K., Bianchi, F., Breitenlechner, M., Brilke, S.,

672   Chen, X., Craven, J. S., Dias, A., Ehrhart, S., Fischer, L., Flagan, R. C., Franchin, A., Fuchs,

673   C., Guida, R., Hakala, J., Hoyle, C. R., Jokinen, T., Junninen, H., Kangasluoma, J., Kim, J.,

674   Kirkby, J., Krapf, M., Kürten, A., Laaksonen, A., Lehtipalo, K., Makhmutov, V., Mathot, S.,

675   Molteni, U., Monks, S. A., Onnela, A., Peräkylä, O., Piel, F., Petäjä, T., Praplan, A. P., Pringle,

K. J., Richards, N. A. D., Rissanen, M. P., Rondo, L., Sarnela, N., Schobesberger, S., Scott, C. E., Seinfeld, J. H., Sharma, S., Sipilä, M., Steiner, G., Stozhkov, Y., Stratmann, F., Tomé, A., Virtanen, A., Vogel, A. L., Wagner, A. C., Wagner, P. E., Weingartner, E., Wimmer, D., Winkler, P. M., Ye, P., Zhang, X., Hansel, A., Dom- men, J., Donahue, N. M., Worsnop, D. R., Baltensperger, U., Kulmala, M., Curtius, J., and Carslaw, K. S.: Reduced anthropogenic aerosol radiative forcing caused by biogenic new particle formation, P. Natl. Acad. Sci. USA, 113, 12053–12058, 2016.

Guenther, A., Karl, T., Harley, P., Wiedinmyer, C., Palmer, P. I., and Geron, C.: Estimates of global terrestrial isoprene emissions using MEGAN (Model of Emissions of Gases and Aerosols from Nature), Atmos. Chem. Phys., 6, 3181–3210, 2006.

Hallquist, M., Wenger, J. C., Baltensperger, U., Rudich, Y., Simpson, D., Claeys, M., Dommen, J., Donahue, N. M., George, C., Goldstein, a. H., Hamilton, J. F., Herrmann, H., Hoffmann, T., Iinuma, Y., Jang, M., Jenkin, M. E., Jimenez, J. L., Kiendler-Scharr, a., Maenhaut, W., McFiggans, G., Mentel, T. F., Monod, A., Prévôt, A. S. H., Seinfeld, J. H., Surratt, J. D., Szmigielski, R. and Wildt, J.: The formation, properties and impact of secondary organic aerosol: current and emerging issues, Atmos. Chem. Phys., 9, 5155–5236, 2009.

Hamed, A., Joutsensaari, J., Mikkonen, S., Sogacheva, L., Dal Maso, M., Kulmala, M., Cavalli, F., Fuzzi, S., Facchini, M. C., Decesari, S., Mircea, M., Lehtinen, K. E. J., and Laaksonen, A.: Nucleation and growth of new particles in Po Valley, Italy, Atmos. Chem. Phys., 7, 355–376, 2007.

Im, U., Markakis, K., Unal, A., Kindap, T., Poupkou, A., Incecik, S., Yenigun, O., Melas, D., Theodosi, C., and Mihalopoulos, N.: Study of a winter PM episode in Istanbul using the high resolution WRF/CMAQ modeling system, Atmos. Environ., 44, 3085–3094, 2010.

Jimenez-Guerrero, P., Jorba, O., Baldasano, J. M., and Gasso, S.: The use of a modelling system as a tool for air quality management: Annual high-resolution simulations and evaluation, Sci. Total Environ., 390, 323–340, 2008.

Jokinen, T., Berndt, T., Makkonen, R., Kerminen, V.-M., Jun- ninen, H., Paasonen, P., Stratmann, F., Herrmann, H., Guenther, A. B., Worsnop, D. R., Kulmala, M., Ehn, M., and Sipilä, M.: Production of extremely low volatile organic com- pounds from biogenic emissions: Measured yields and atmospheric implications, P. Natl. Acad. Sci. USA, 112, 7123–7128, 2015.

706 Jung, J., Adams, P. J., and Pandis, S. N.: Simulating the size distribution and chemical composition
707   of ultrafine particles during nucleation events, Atmos. Environ., 40, 2248–2259, 2006.

708 Jung, J. G., Fountoukis, C., Adams, P. J. and Pandis, S. N.: Simulation of in situ ultrafine particle
709   formation in the eastern United States using PMCAMx-UF, J. Geophys. Res., 115, D03203,
710   doi: 10.1029/2009jd012313, 2010.

711 Kanakidou, M., Seinfeld, J. H., Pandis, S. N., Barnes, I., Dentener, F. J., Facchini, M. C., Van
712   Dingenen, R., Ervens, B., Nenes, A., Nielsen, C. J., Swietlicki, E., Putaud, J. P., Balkanski, Y.,
713   Fuzzi, S., Horth, J., Moortgat, G. K., Winterhalter, R., Myhre, C. E. L., Tsigaridis, K., Vignati,
714   E., Stephanou, E. G., and Wilson, J.: Organic aerosol and global climate modelling: a review,
715   Atmos. Chem. Phys., 5, 1053–1123, 2005.

716 Karydis, V. A., Tsimpidi, A. P., and Pandis, S. N.: Evaluation of a three-dimensional chemical
717   transport model (PMCAMx) in the eastern United States for all four seasons, J. Geophys. Res.,
718   112, D14211, https://doi.org/10.1029/2006JD007890, 2007.

719 Kirkby, J., Duplissy, J., Sengupta, K., Frege, C., Gordon, H., Williamson, C., Heinritzi, M., Simon,
720   M., Yan, C., Almeida, J., Tröstl, J., Nieminen, T., Ortega, I. K., Wagner, R., Adamov, A.,
721   Amorim, A., Bernhammer, A.-K., Bianchi, F., Breitenlechner, M., Brilke, S., Chen, X.,
722   Craven, J., Dias, A., Ehrhart, S., Flagan, R. C., Franchin, A., Fuchs, C., Guida, R., Hakala, J.,
723   Hoyle, C. R., Jokinen, T., Junninen, H., Kangasluoma, J., Kim, J., Krapf, M., Kürten, A.,
724   Laaksonen, A., Lehtipalo, K., Makhmutov, V., Mathot, S., Molteni, U., Onnela, A., Peräkylä,
725   O., Piel, F., Petäjä, T., Praplan, A. P., Pringle, K., Rap, A., Richards, N. A. D., Riip- inen, I.,
726   Rissanen, M. P., Rondo, L., Sarnela, N., Schobesberger, S., Scott, C. E., Seinfeld, J. H., Sipilä,
727   M., Steiner, G., Stozhkov, Y., Stratmann, F., Tomé, A., Virtanen, A., Vogel, A. L., Wag- ner,
728   A. C., Wagner, P. E., Weingartner, E., Wimmer, D., Winkler, P. M., Ye, P., Zhang, X., Hansel,
729   A., Dommen, J., Donahue, N. M., Worsnop, D. R., Baltensperger, U., Kulmala, M., Carslaw,
730   K. S., and Curtius, J.: Ion-induced nucleation of pure biogenic particles, Nature, 533, 521–526,
731   https://doi.org/10.1038/nature17953, 2016.

732 Kleinman, L. I., Springston, S. R., Daum, P. H., Lee, Y.-N., Nunnermacker, L. J., Senum, G. I.,
733   Wang, J., Weinstein-Lloyd, J., Alexander, M. L., Hubbe, J., Ortega, J., Canagaratna, M. R.,
734   and Jayne, J.: The time evolution of aerosol composition over the Mexico City plateau, Atmos.
735   Chem. Phys., 8, 1559–1575, doi:10.5194/acp-8-1559-2008, 2008.

Kostenidou, E., Florou, K., Kaltsonoudis, C., Tsiflikiotou, M., Vratolis, S., Eleftheriadis, K., and Pandis, S. N.: Sources and chemical characterization of organic aerosol during the summer in the eastern Mediterranean, Atmos. Chem. Phys., 15, 11355–11371, 2015.

Kroll, J. H., Ng, N. L., Murphy, S. M., Flagan, R. C., Seinfeld, J. H.: Secondary organic aerosol formation from isoprene photooxidation, Environ. Sci. Technol., 40, 155-162, 2006.

Kulmala, M., Vehkamaki, H., Petaja, T., Dal Maso, M., Lauri, A., Kerminen, V.-M, Birmili, W., and McMurry, P. H.: Formation and growth of ultrafine atmospheric particles: A review of observations, J. Aerosol Sci., 35, 143–176, 2004.

Kulmala, M., Asmi, A., Lappalainen, H. K., Baltensperger, U., Brenguier, J.-L., Facchini, M. C., Hansson, H.-C., Hov, Ø., O'Dowd, C. D., Pöschl, U., Wiedensohler, A., Boers, R., Ammann, M., Arabas, S., Artaxo, P., Baars, H., Beddows, D. C. S., Bergström, R., Beukes, J. P., Bilde, M., Burkhart, J. F., Canonaco, F., Clegg, S. L., Coe, H., Crumeyrolle, S., D'Anna, B., Decesari, S., Gilardoni, S., Fischer, M., Fjaeraa, A. M., Fountoukis, C., George, C., Gomes, L., Halloran, P., Hamburger, T., Harrison, R. M., Herrmann, H., Hoffmann, T., Hoose, C., Hu, M., Hyvärinen, A., Hõrrak, U., Iinuma, Y., Iversen, T., Josipovic, M., Kanakidou, M., Kiendler-Scharr, A., Kirkevåg, A., Kiss, G., Klimont, Z., Kolmonen, P., Komppula, M., Kristjánsson, J.-E., Laakso, L., Laaksonen, A., Labonnote, L., Lanz, V. A., Lehtinen, K. E. J., Rizzo, L. V., Makkonen, R., Manninen, H. E., McMeeking, G., Merikanto, J., Minikin, A., Mirme, S., Morgan, W. T., Nemitz, E., O'Donnell, D., Panwar, T. S., Pawlowska, H., Petzold, A., Pienaar, J. J., Pio, C., Plass-Duelmer, C., Prévôt, A. S. H., Pryor, S., Reddington, C. L., Roberts, G., Rosen- feld, D., Schwarz, J., Seland, Ø., Sellegri, K., Shen, X. J., Shiraiwa, M., Siebert, H., Sierau, B., Simpson, D., Sun, J. Y., Topping, D., Tunved, P., Vaattovaara, P., Vakkari, V., Veefkind, J. P., Visschedijk, A., Vuollekoski, H., Vuolo, R., Wehner, B., Wildt, J., Woodward, S., Worsnop, D. R., van Zadelhoff, G.- J., Zardini, A. A., Zhang, K., van Zyl, P. G., Kerminen, V.- M., S Carslaw, K., and Pandis, S. N.: General overview: Euro- pean Integrated project on Aerosol Cloud Climate and Air Quality interactions (EUCAARI) – integrating aerosol research from nano to global scales, Atmos. Chem. Phys., 11, 13061–13143, https://doi.org/10.5194/acp-11-13061-2011, 2011.

Lampilahti, J., Manninen, H. E., Nieminen, T., Mirme, S., Ehn, M., Pullinen, I., Leino, K., Schobesberger, S., Kangasluoma, J., Kontkanen, J., Järvinen, E., Väänänen, R., Yli-Juuti, T., Krejci, R., Lehtipalo, K., Levula, J., Mirme, A., Decesari, S., Tillmann, R., Worsnop, D. R.,

Rohrer, F., Kiendler-Scharr, A., Petäjä, T., Kerminen, V.-M., Mentel, T. F., and Kulmala, M.: Zeppelin-led study on the onset of new particle formation in the planetary boundary layer, Atmos. Chem. Phys. Discuss. [preprint], https://doi.org/10.5194/acp-2021-282, in review, 2021.

Lane, T. E., Donahue, N. M., and Pandis, S. N.: Simulating secondary organic aerosol formation using the volatility basis-set approach in a chemical transport model, Atmos. Environ., 42, 7439–7451, 2008.

Makkonen, R., Asmi, A., Korhonen, H., Kokkola, H., Järvenoja, S., Räisänen, P., Lehtinen, K. E. J., Laaksonen, A., Kerminen, V.- M., Järvinen, H., Lohmann, U., Bennartz, R., Feichter, J., and Kulmala, M.: Sensitivity of aerosol concentrations and cloud properties to nucleation and secondary organic distribution in ECHAM5-HAM global circulation model, Atmos. Chem. Phys., 9, 1747–1766, https://doi.org/10.5194/acp-9-1747-2009, 2009.

Mann, G. W., Carslaw, K. S., Spracklen, D. V., Ridley, D. A., Manketelow, P. T., Chipperfield, M. P., Pickering, S. J., and Johnson, C. E.: Description and evaluation of GLOMAP-mode: A modal global aerosol microphysics model for the UKCA composition-climate model. Geosci. Model Dev., 3, 519-551, 2010.

Matsui, H., et al.: Secondary organic aerosol formation in urban air: Temporal variations and possible contributions from unidentified hydrocarbons, J. Geophys. Res., 114, D04201, doi:10.1029/2008JD010164, 2009.

Merikanto, J., Spracklen, D. V., Mann, G. W., Pickering, S. J., and Carslaw, K. S.: Impact of nucleation on global CCN, Atmos. Chem. Phys., 9, 8601–8616, https://doi.org/10.5194/acp-9-8601- 2009, 2009.

Mikuška, P., Večeřa, Z., Bartošíková, A., Maenhaut, W.: Annular diffusion denuder for simultaneous removal of gaseous organic compounds and air oxidants during sampling of carbonaceous aerosols, Anal Chim Acta., 714, 68-75. 2012.Murphy, B. N., Pandis, S. N. and Ave, F.: Simulating the formation of semivolatile primary and secondary organic aerosol in a regional chemical transport model gas-phase chemistry of OA species, Environ. Sci. Technol., 43, 4722–4728, 2009.

Napari, I., Noppel, M., Vehkamaki, H., and Kulmala, M.: Parameterization of ternary nucleation rates for H_2SO_4-NH_3-H_2O vapors, J. Geophys. Res., 107, AAC 6-1–AAC 6-6, https://doi.org/10.1029/2002JD002132, 2002.

798 Ng, N. L., Kroll, J. H., Keywood, M. D., Bahreini, R., Varutbangkul, V., Flagan, R. C., Seinfeld,
799   J. H.: Contribution of first- versus second-generation products to secondary organic aerosols
800   formed in the oxidation of biogenic hydrocarbons, Environ. Sci. Technol., 40, 2283-2297,
801   2006.

802 Nenes, A., Pandis, S. N., and Pilinis, C.: ISORROPIA: a new thermodynamic equilibrium model
803   for multiphase multicomponent inorganic aerosols, Aquat. Geochem., 4, 123–152, 1998.

804 Odum, J. R., Hoffmann, T., Bowman, F. A., Collins, D., Flagan, R. C., Seinfeld, J. H.: Gas/particle
805   partitioning and secondary organic aerosol yields, Environ. Sci. Technol., 30, 2580-2585,
806   1996.

807 O'Dowd, C. D., Langmann, B., Varghese, S., Scannell, C., Ceburnis, D., and Facchini, M. C.: A
808   combined organic-inorganic sea-spray source function, Geophys. Res. Lett., 35, L01801,
809   https://doi.org/10.1029/2007GL030331, 2008.

810 Olenius, T., Yli-Juuti, T., Elm, J, Kontkanen, J., and Riipinen I. New particle formation and
811   growth: creating a new atmospheric phase interface. In Physical Chemistry of Gas-Liquid
812   Interfaces (eds. Faust, J. A. & House, J. E.), 315–352, Elsevier, 2018.

813 Pandis, S. N., Wexler, A. S., and Seinfeld, J. H.: Secondary organic aerosol formation and
814   transport. 2. Predicting the ambient secondary organic aerosol size distribution, Atmos.
815   Environ., 27A, 2403–2416, 1993.

816 Pathak, R. K., Presto, A. A., Lane, T. E., Stanier, C. O., Donahue, N. M., Pandis, S. N.: Ozonolysis
817   of α-pinene: parameterization of secondary organic aerosol mass fraction, Atmos. Chem.
818   Phys., 7, 3811–3821, 2007.

819 Patoulias, D., Fountoukis, C., Riipinen, I., and Pandis, S. N.: The role of organic condensation on
820   ultrafine particle growth during nucleation events, Atmos. Chem. Phys., 15, 6337–6350,
821   https://doi.org/10.5194/acp-15-6337-2015, 2015.

822 Patoulias, D., Fountoukis, C., Riipinen, I., Asmi, A., Kulmala, M., and Pandis, S. N.: Simulation
823   of the size-composition distribution of atmospheric nanoparticles over Europe, Atmos. Chem.
824   Phys., 18, 13639–13654, https://doi.org/10.5194/acp-18-13639-2018, 2018.

825 Pierce, J. R. and Adams, P. J.: A computationally efficient aerosol nucleation/condensation
826   method: Pseudo-steady state sulfuric acid, Aerosol Sci. Tech., 43, 216–226, 2009

827 Pierce, J. R., Riipinen, I., Kulmala, M., Ehn, M., Petäjä, T., Junninen, H., Worsnop, D. R., and
828   Donahue, N. M.: Quantification of the volatility of secondary organic compounds in ultrafine

particles during nucleation events, Atmos. Chem. Phys., 11, 9019–9036, https://doi.org/10.5194/acp-11-9019-2011, 2011.

Presto, A. A., Donahue, N. M.: Investigation of a-pinene+ozone secondary organic aerosol formation at low total aerosol mass. Environ. Sci. Technol., 40, 3536–3543, 2006.

Rissanen, M. P., Kurtén, T., Sipilä, M., Thornton, J. A., Kangasluoma, J., Sarnela, N., Junninen, H., Jørgensen, S., Schallhart, S., Kajos, M. K., Taipale, R., Springer, M., Mentel, T. F., Ruuska-nen, T., Petäjä, T., Worsnop, D. R., Kjaergaard, H. G., and Ehn, M.: The formation of highly oxidized multifunctional products in the ozonolysis of cyclohexene, J. Am. Chem. Soc., 136, 15596–15606, 2014.

Robinson, A. L., Donahue, N. M., Shrivastava, M. K., Weitkamp, E. A., Sage, A. M., Grieshop, A. P., Lane, T. E., Pandis, S. N., Pierce, J. R.: Rethinking organic aerosols: semivolatile emissions and photochemical aging, Science, 315, 1259-1262, 2007.

Schulze, B. C., Wallace, H. W., Flynn, J. H., Lefer, B. L., Erickson, M. H., Jobson, B. T., Dusanter, S., Griffith, S. M., Hansen, R. F., Stevens, P. S., VanReken, T., and Griffin, R. J.: Differences in BVOC oxidation and SOA formation above and below the forest canopy, Atmos. Chem. Phys., 17, 1805–1828, https://doi.org/10.5194/acp-17-1805-2017, 2017.

Seinfeld, J. H.; Pandis S. N. Atmospheric Chemistry and Physics: From Air Pollution to Climate Change, 2nd ed.; John Wiley and Sons, Hoboken, NJ, 2006.

Sengupta, K., Pringle, K., Johnson, J. S., Reddington, C., Browse, J., Scott, C. E., and Carslaw, K.: A global model perturbed parameter ensemble study of secondary organic aerosol formation, Atmos. Chem. Phys., 21, 2693–2723, https://doi.org/10.5194/acp-21-2693-2021, 2021.

Shrivastava, M. K., Lane, T. E., Donahue, N. M., Pandis, S. N., and Robinson, A. L.: Effects of gas-particle partitioning and aging of primary emissions on urban and regional organic aerosol concentrations, J. Geophys. Res., 113, D18301, doi:10.1029/2007JD009735, 2008.

Shrivastava, M., Thornton, J., Cappa, C., Fan, J., Goldstein, A., Guenther, A., Jimenez, J. L., Kuang, C., Laskin, A., Martin, S., Ng, N. L., Petaja, T., Pierce, J., Rasch, P., Roldin, P., Seinfeld, J., Shilling, J., Smith, J., Volkamer, R., Wang, J., Worsnop, D., Zaveri, R., Zelenyuk, A., and Zhang, Q.: Recent advances in understanding secondary organic aerosols: implications for global climate forcing, Rev. Geophys., 55, 509-559, 2017.

859   Skamarock, W. C., Klemp, J. B., Dudhia, J., Gill, D. O., Barker, D. M., Wang, W., and Powers, J.
860   G.: A Description of the Advanced Research WRF Version 2, NCAR Technical Note, available
861   at: http://www2.mmm.ucar.edu/wrf/users/docs/arw_v2_070111.pdf (last access: 12
862   September 2018), 2005.

863   Sofiev, M., Vankevich, R., Lanne, M., Koskinen, J., and Kukkonen, J.: On integration of a Fire
864   Assimilation System and a chemical transport model for near-real-time monitoring of the
865   impact of wild-land fires on atmospheric composition and air quality, Modelling, Monitoring
866   and Management of Forest Fires, WIT Trans. Ecol. Envir., 119, 343–351, 2008a.

867   Sofiev, M., Lanne, M., Vankevich, R., Prank, M., Karppinen, A., and Kukkonen, J.: Impact of
868   wild-land fires on European air quality in 2006–2008, Modelling, Monitoring and Management
869   of Forest Fires, WIT Trans. Ecol. Envir., 119, 353–361, 2008b.

870   Sogacheva, L., Hamed, A., Facchini, M. C., Kulmala, M., and Laaksonen, A.: Relation of air mass
871   history to nucleation events in Po Valley, Italy, using back trajectories analysis, Atmos. Chem.
872   Phys., 7, 839–853, https://doi.org/10.5194/acp-7-839-2007, 2007.

873   Spracklen, D. V., Pringle, K. J., Carslaw, K. S., Chipperfield, M. P., and Mann, G. W.: A global
874   off-line model of size- resolved aerosol microphysics: I. Model development and prediction of
875   aerosol properties, Atmos. Chem. Phys., 5, 2227– 2252, doi:10.5194/acp-5-2227-2005, 2005.

876   Stanier, C. O., Pathak, R. K. and Pandis, S. N.: Measurements of the volatility of aerosols from a-
877   pinene ozonolysis, Environ. Sci. Technol., 41, 2756–2763, 2007.

878   Turpin, B. J., Saxena, P., and Andrews, E.: Measuring and simulating particulate organics in the
879   atmosphere: problems and prospects, Atmos. Environ., 34, 2983-3013, 2000.

880   Vehkamäki, H., Kulmala, M., Napari, I., Lehtinen, K. E. J., Timmreck, C., Noppel, M., and
881   Laaksonen, A.: An improved parameterization for sulfuric acid-water nucleation rates for
882   tropospheric and stratospheric conditions, J. Geophys. Res., 107, 4622–4632, 2002.

883   Visschedijk, A. J. H., Zandveld, P., and Denier van der Gon, H. A. C.: TNO Report 2007 A-
884   R0233/B: A high resolution gridded European emission database for the EU integrated project
885   GEMS, Organization for Applied Scientific Research, the Netherlands, 2007.

886   Volkamer, R., Jimenez, J. L., San Martini, F., et al.: Secondary organic aerosol formation from
887   anthropogenic air pollution: Rapid and higher than expected, Geophys. Res. Lett., 33, L17811,
888   doi:10.1029/2006GL026899, 2006.

889   Wang, M. and Penner, J. E.: Aerosol indirect forcing in a global model with particle nucleation,
890   Atmos. Chem. Phys., 9, 239–260, https://doi.org/10.5194/acp-9-239-2009, 2009.

891   Yli-Juuti, T., Mohr, C., and Riipinen, I. Open questions on atmospheric nanoparticle
892   growth. Commun. Chem. 3, 106, https://doi.org/10.1038/s42004-020-00339-4, 2020.

893   Yu, F. and Luo, G.: Simulation of particle size distribution with a global aerosol model:
894   contribution of nucleation to aerosol and CCN number concentrations, Atmos. Chem. Phys.,
895   9, 7691– 7710, doi:10.5194/acp-9-7691-2009, 2009.

896   Zhang, Q., Jimenez, J. L., Canagaratna, M. R., Allan, J. D., Coe, H., Ulbrich, I., Alfarra, M. R.,
897   Takami, A., Middlebrook, A. M., Sun, Y. L., Dzepina, K., Dunlea, E., Docherty, K., DeCarlo,
898   P. F., Salcedo, D., Onasch, T., Jayne, J. T., Miyoshi, T., Shimono, A., Hatakeyama, S.,
899   Takegawa, N., Kondo, Y., Schneider, J., Drewnick, F., Borrmann, S., Weimer, S., Demerjian,
900   K., Williams, P., Bower, K., Bahreini, R., Cottrell, L., Griffin, R. J., Rautiainen, J., Sun, J. Y.,
901   Zhang, Y. M., and Worsnop, D. R.: Ubiquity and dominance of oxygenated species in organic
902   aerosols in anthropogenically-influenced Northern Hemisphere midlatitudes, Geophys. Res.
903   Lett., 34, L13801, doi:10.1029/2007GL029979, 2007.

904

905

Table 1: Summary of parameters used in each simulation

CASE	Aging of anthropogenic IVOCs and SVOCs	Source of ELVOCs	Emission of IVOCs
1 (Base case)		Monoterpene oxidation 5% molar yield	Yes
2	Aging with OH $k=10^{-11}$ cm^3 molecule^{-1} s^{-1}	None	Yes
3		Monoterpene oxidation 5% molar yield	No

906
907
908
909
910
911
912
913
914
915
916
917
918
919
920
921
922
923
924
925
926
927
928
929
930
931
932
933
934

Table 2: Prediction skill metrics of PMCAMx-UF against daily ground measurements of particle number concentration above 10 nm (N_{10}) during 5 June – 8 July 2012.

Station	Mean Observed (cm^{-3})	Mean Predicted (cm^{-3})		NMB (%)		NME(%)	
		Base case	Without ELVOCs	Base case	Without ELVOCs	Base case	Without ELVOCs
N_{10}							
ANB	8057	6617	6585	-18	-18	39	39
ASP	2130	5233	5202	146	144	144	144
BRK	1878	3144	3053	67	63	86	86
CBW	13101	9913	9817	-24	-25	31	31
DSN	10591	6508	6504	-39	-39	41	41
DSW	7706	6111	6091	-21	-21	40	40
FNK	3962	5466	5466	38	38	40	40
GDN	5712	6652	6731	16	18	32	32
HOH	3438	3070	2906	-11	-15	38	38
HYY	2207	2536	2265	15	3	31	31
ISP	6232	6449	6203	3	0	43	43
KPU	5269	5855	5937	11	13	43	43
KST	3596	4881	4834	36	34	46	46
MLP	5583	6034	6003	8	8	42	42
MNT	6455	8364	8273	30	28	45	45
PRG	7272	7281	7273	0	0	44	44
USM	15171	8335	8413	-45	-45	52	52
VAV	3250	8291	8283	155	155	155	155
VRR	1107	1491	1190	35	7	69	57
VSM	2903	7281	7011	151	141	151	141
WLD	4956	7903	7783	59	57	66	64
ZUG	1237	2405	2287	94	85	111	103
NEO	2864	5085	5039	78	76	79	78
PAT	4705	5151	5148	9	9	45	44
SPC	8301	7198	7180	-13	-14	35	35
THE	3894	8577	8530	120	119	120	119
ALL	**4820**	**5957**	**5889**	**23**	**22**	**63**	**63**

942 **Table 3:** Prediction skill metrics of PMCAMx-UF against daily ground measurements of particle
943 number concentration above 100 nm (N_{100}) during 5 June – 8 July 2012.
944

Station	Mean Observed (cm^{-3})	Mean Predicted (cm^{-3})		NMB (%)		NME(%)	
		Base case	Without ELVOCs	Base case	Without ELVOCs	Base case	Without ELVOCs
N_{100}							
ANB	1518	939	934	-38	-38	47	47
ASP	552	789	694	43	26	61	51
BRK	607	419	397	-31	-35	65	62
CBW	1627	1550	1441	-5	-11	18	16
DSN	1976	1178	1052	-40	-47	44	49
DSW	1426	1156	1050	-19	-26	35	37
FNK	1760	2383	2330	35	32	39	36
GDN	2492	2797	2826	12	13	34	33
HOH	1011	697	656	-31	-35	37	40
HYY	677	579	445	-14	-34	26	38
ISP	1775	1334	1283	-25	-28	37	38
KPU	1543	1898	1861	23	21	29	28
KST	1123	1138	1061	1	-6	26	21
MLP	1214	1111	977	-9	-20	30	33
MNT	1492	1871	1799	25	21	49	50
PRG	1177	1256	1167	7	-1	26	25
USM	1657	1091	985	-34	-41	40	44
VAV	766	942	899	23	17	48	48
VRR	324	166	90	-49	-72	63	77
VSM	704	747	643	6	-9	34	34
WLD	1116	1063	955	-5	-14	20	23
ZUG	555	555	546	0	-2	44	44
NEO	1489	2041	1971	37	32	45	42
PAT	1747	1765	1766	1	1	21	23
SPC	1702	2051	1978	21	16	36	36
THE	1387	2420	2384	74	72	78	76
ALL	**1198**	**1326**	**1258**	**10**	**5**	**45**	**45**

945

946

947

948

949 **Table 4:** Predicted (PMCAMx-UF) and observed (AMS) average PM_1 concentrations of sulfate,

950 ammonium and nitrate in different locations for base case simulation.

Station	Sulfate		Ammonium		Nitrate	
	Predicted ($\mu g\ m^{-3}$)	Observed ($\mu g\ m^{-3}$)	Predicted ($\mu g\ m^{-3}$)	Observed ($\mu g\ m^{-3}$)	Predicted ($\mu g\ m^{-3}$)	Observed ($\mu g\ m^{-3}$)
FIN	4.44	3.50	1.82	1.06	1.00	0.07
PAT	2.83	3.35	1.34	0.95	0.84	0.10
BOL	2.11	2.79	1.08	1.00	0.90	0.60
SPC	2.31	1.81	1.16	0.88	0.99	1.20
ALL	2.99	2.82	1.37	0.97	0.94	0.52

951

952

953

954

955

956

957

958

959

960

961

962

963

964

965

966

967 **Table 5:** Prediction skill metrics of PMCAMx-UF base case simulation against daily PM_1 OA
968 measurements.

Station	Mean Predicted ($\mu g\ m^{-3}$)	Mean Observed ($\mu g\ m^{-3}$)	NMB (%)	NME (%)	Factor of 2 (%)
FIN	3.19	2.12	50	51	83
PAT	2.75	3.80	-28	28	95
BOL	4.62	5.68	-19	33	74
SPC	4.74	3.98	19	44	77
ALL	3.87	3.79	2	38	82

969
970

971 **Table 6:** Prediction skill metrics of PMCAMx-UF against daily PM$_{2.5}$ OA measurements.

Name	Station	Country	Mean Observed ($\mu g\ m^{-3}$)	Mean Predicted ($\mu g\ m^{-3}$)	NMB (%)	NME (%)	Factor of 2 (%)
CH02	Payerne	Switzerland	2.54	2.98	17	73	72
DE44	Melpitz	Germany	2.52	4.42	76	88	66
ES1778	Montseny	Spain	4.52	6.28	39	89	59
IT04	Ispra	Italy	5.13	4.41	-14	46	71
PL05	Diabla Gora	Poland	3.64	4.22	16	43	84
SI08	Iskrba	Slovenia	5.98	5.07	-15	33	80
ALL			**4.06**	**4.56**	**20**	**62**	**72**

972
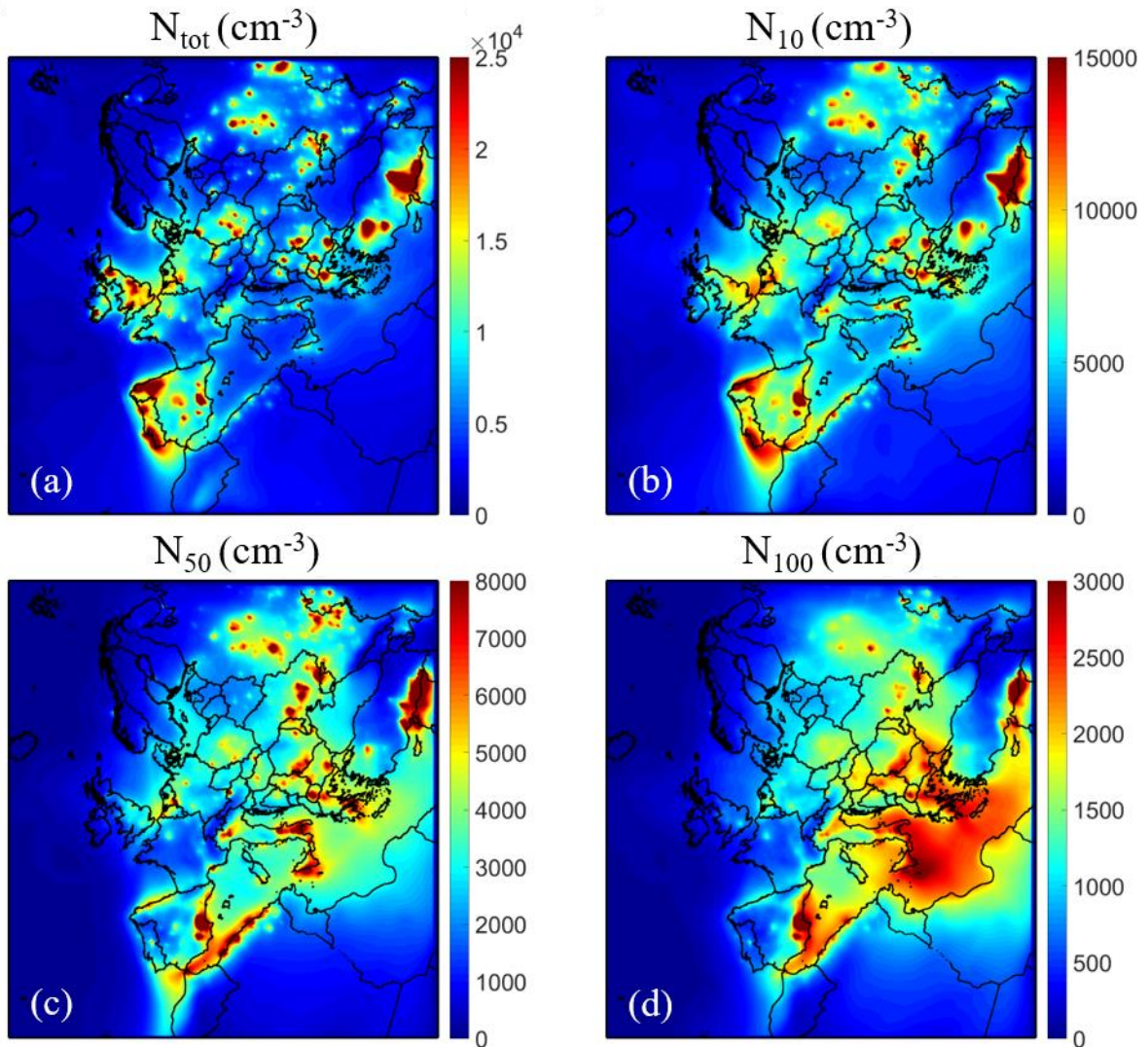
Figure 1: Average ground level number concentrations (in cm^{-3}) for the base case simulation during 5 June – 8 July 2012 for: (a) all particles (N_{tot}); and particles above (b) 10 nm (N_{10}); (c) 50 nm (N_{50}); and (d) 100 nm (N_{100}). Different scales are used.
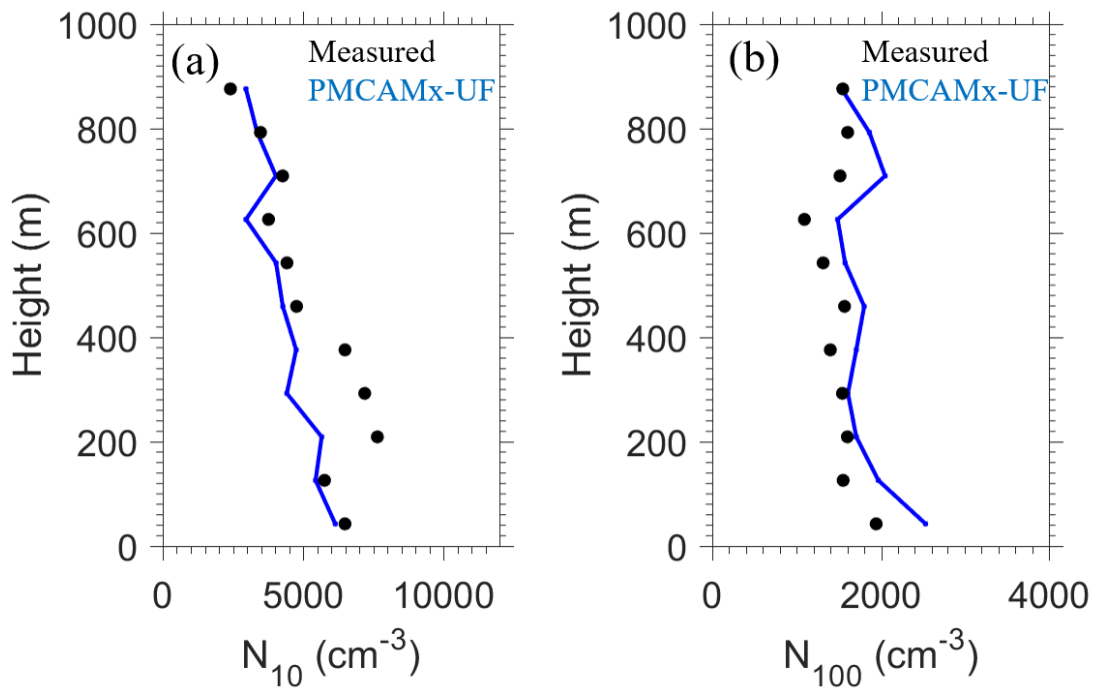
Figure 2: Comparison of predicted PMCAMx-UF (blue line) vs. observed (black dots) vertical profiles of averaged particle number concentrations for (a) N_{10} and (b) N_{100} of 25 flights over the Po Valley during the PEGASOS campaign.

982

ELVOCs PM$_{2.5}$ (μg m^{-3})   ELVOCs/OA PM$_{2.5}$

983
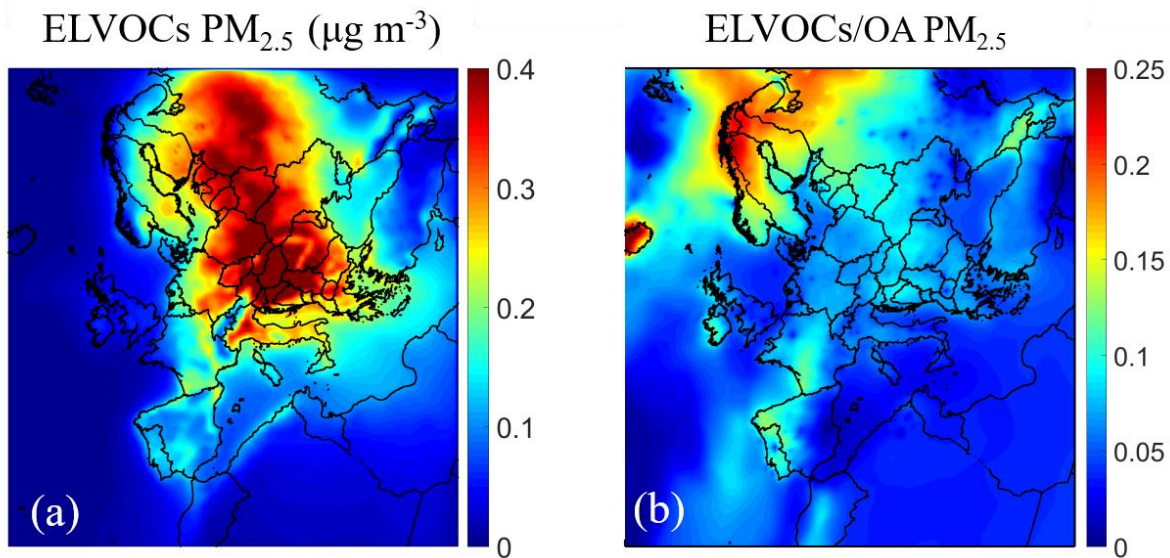
Figure 3: Average ground level (a) PM$_{2.5}$ ELVOCs mass concentration (in μg m^{-3}) and (b) the ratio of the PM$_{2.5}$ mass of ELVOCs to OA during the simulation. Different scales are used.

986
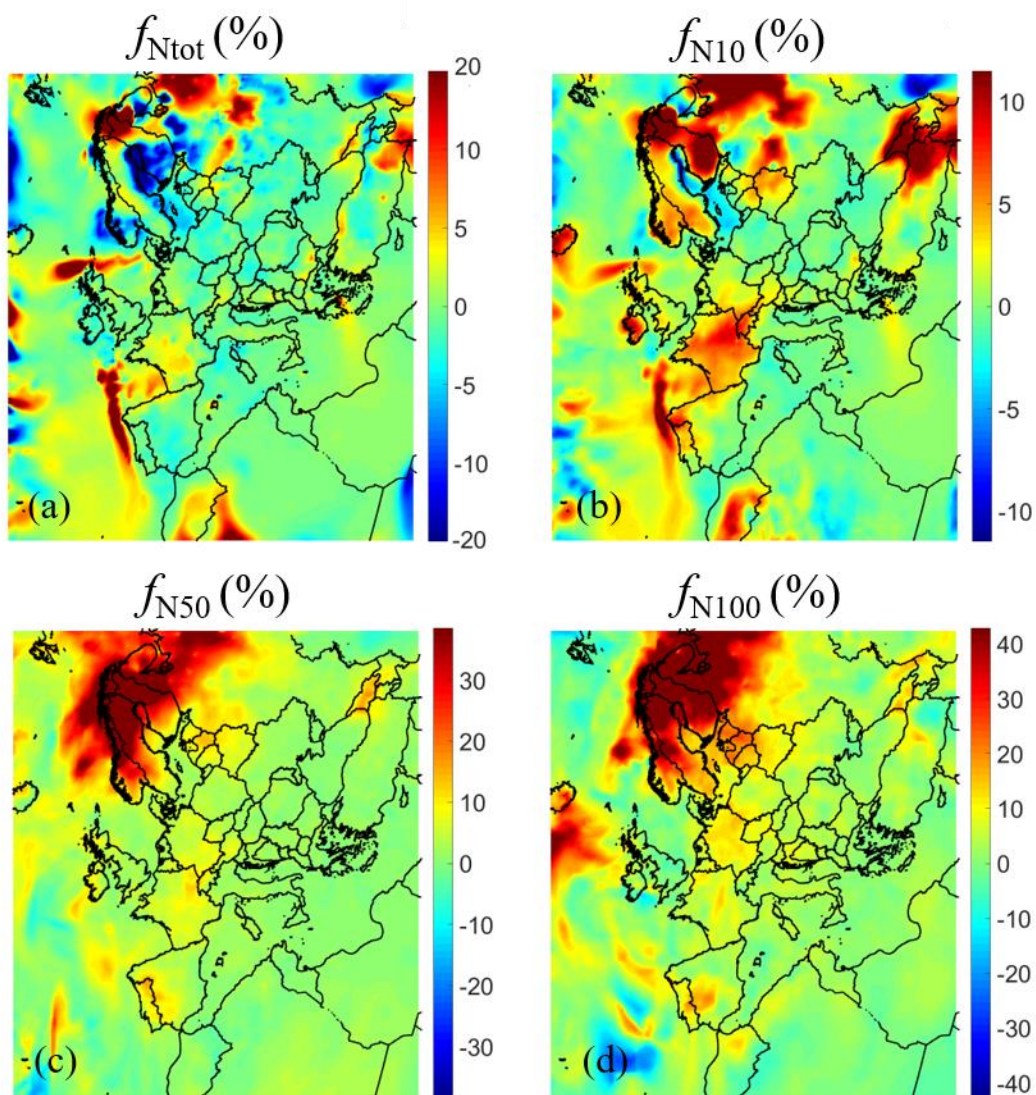
Figure 4: Average ground level fractional increase (f_{Nx}) of number concentration due to the condensation of ELVOCs for: (a) all particles (f_{Ntot}); (b) particles above 10 nm (f_{N10}); (c) above 50 nm (f_{N50}); and (d) above 100 nm (f_{N100}). Different scales are used.

997
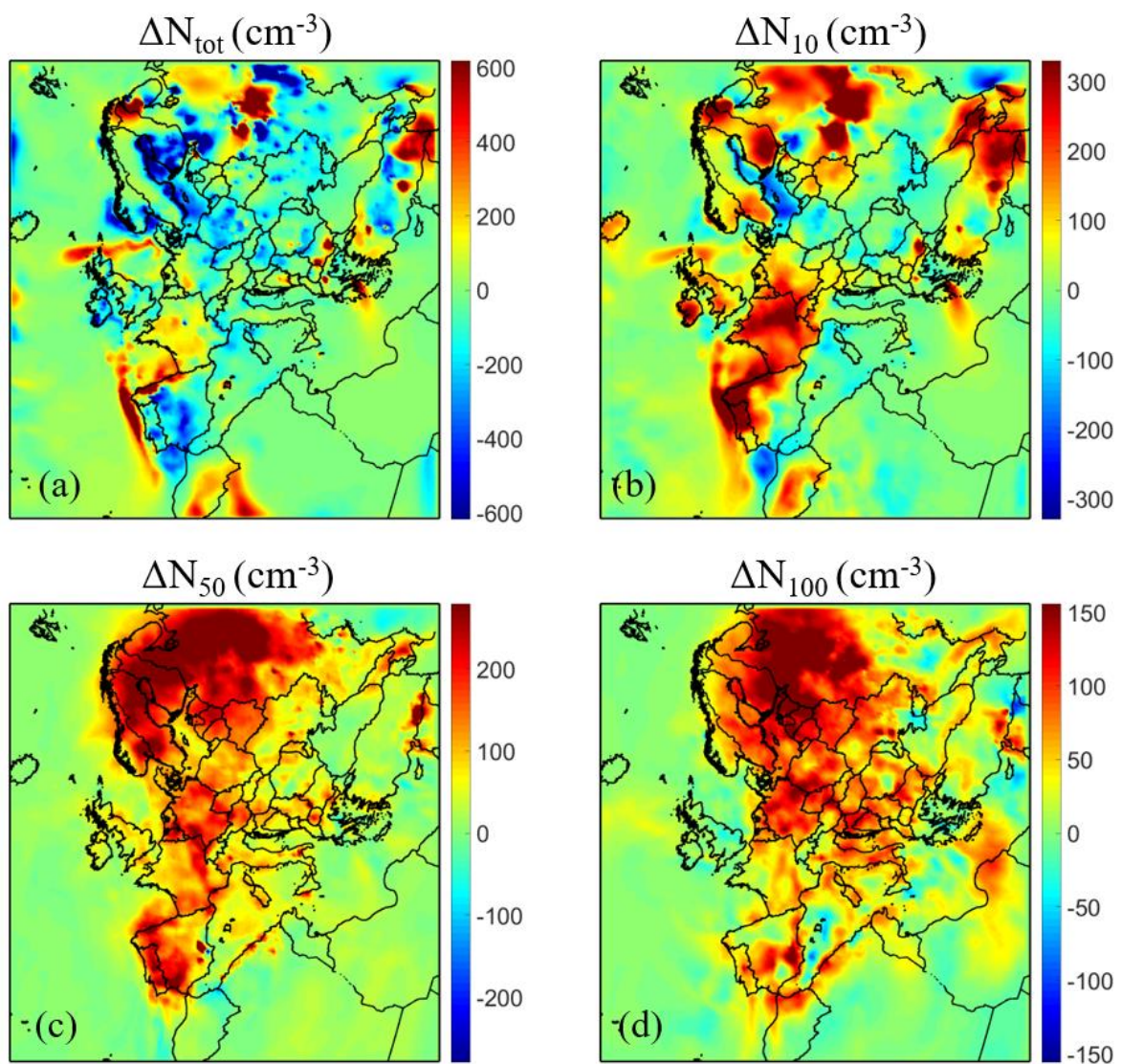
Figure 5: Average ground level increase of number concentration (in cm^{-3}) due to the condensation of ELVOCs for: (a) all particles (ΔN_{tot}); particles above (b) 10 nm (ΔN_{10}); (c) 50 nm (ΔN_{50}); and (d) 100 nm (ΔN_{100}). Different scales are used.

998
999
1000
1001
1002
1003
1004
1005
1006
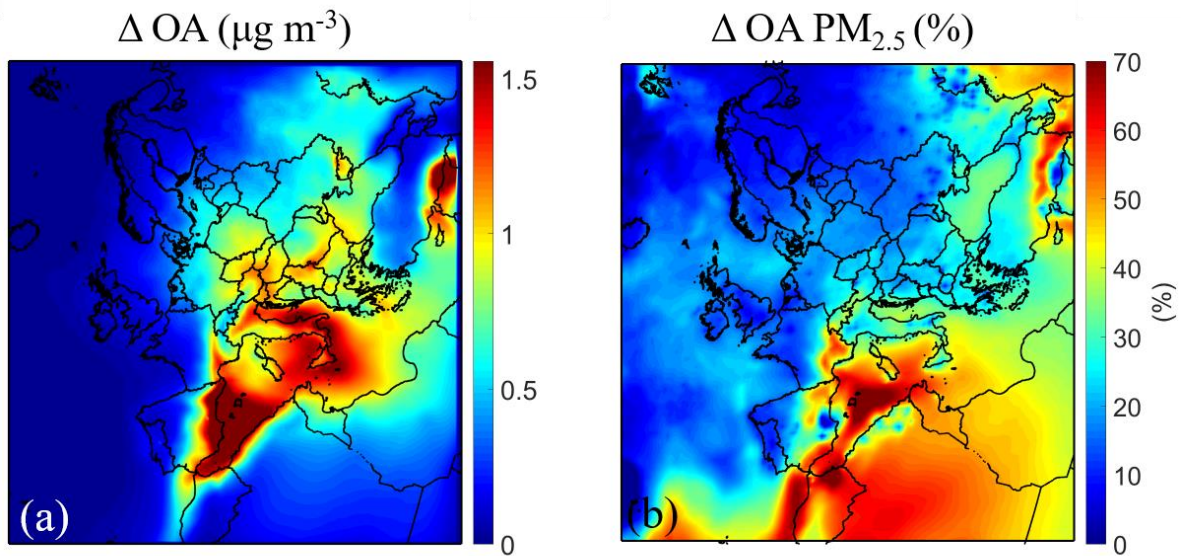
Figure 6: Ground level average (a) increase of PM$_{2.5}$ mass concentration of organics aerosol (in µg m^{-3}) and (b) fractional increase of PM$_{2.5}$ mass concentration of organics aerosol (%) due to the addition of IVOCs emissions of semi-volatility organic aging, predicted during 5 June – 8 July. Different scales are used.
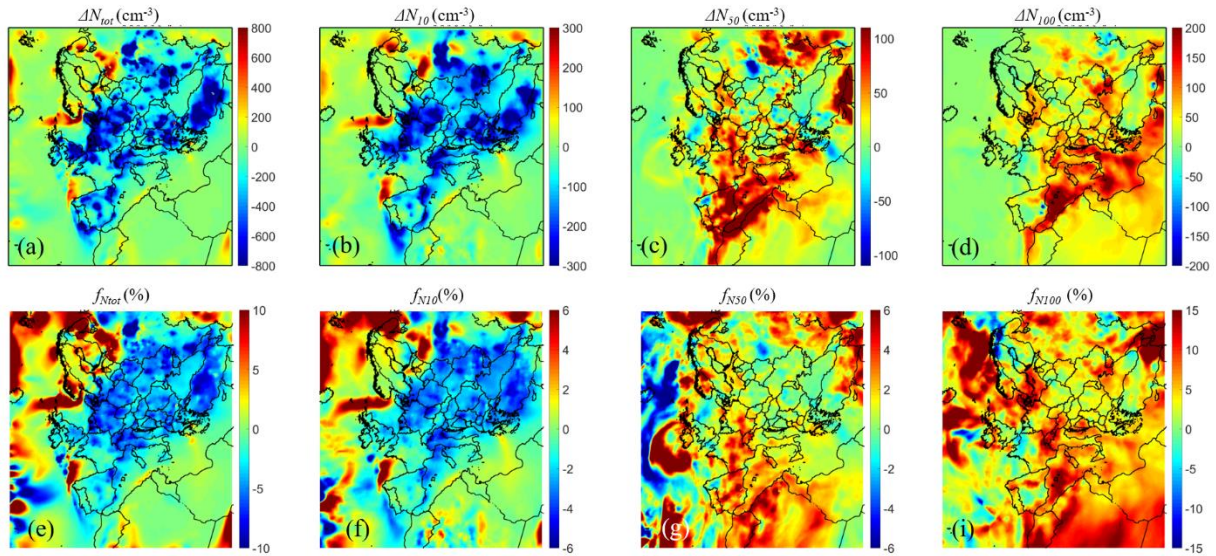
1024

Figure 7: Ground level increase of number concentration (in cm^{-3}) (a-d) and fractional increase ($f_{\text{N}x}$) of number concentration (e-i) due to the addition of IVOCs emissions and aging reactions, predicted during 5 June – 8 July 2012 for: (a, e) all particles (N_{tot}); and particles above (b, f) 10 nm (N_{10}); (c, g) 50 nm (N_{50}); and (d, i) 100 nm (N_{100}). Different scales are used.

1025
1026
1027
1028
1029
1030
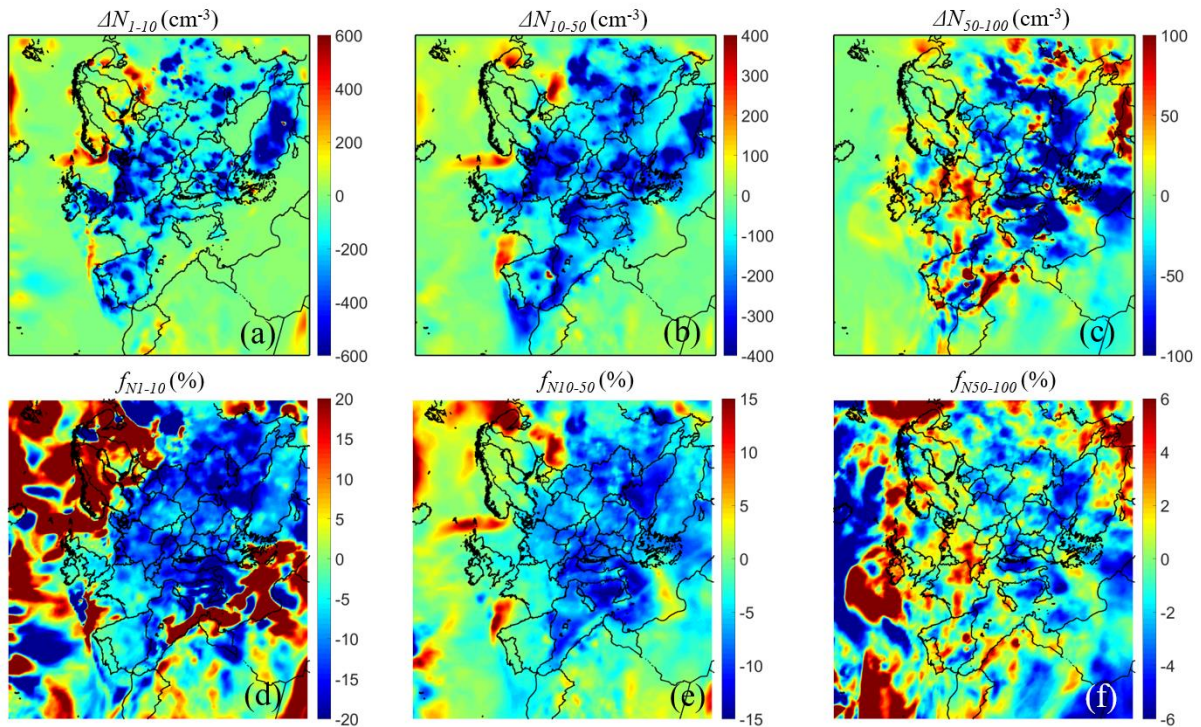
1031

Figure 8: Ground level average increase of number concentration (in cm^{-3}) (a-b-c) and fractional increase (f_{Nx}) of number concentration (d-e-f) due to the addition of IVOCs emissions predicted during 5 June – 8 July 2012 for: (a, d) particles between 0.8 nm and 10 nm (N_{1-10}); (b, e) particles between 10 nm and 50 nm (N_{10-50}) and (c, f) particles between 50 nm and 100 nm (N_{50-100}). Different scales are used.